

April 5, 2024

Concerning the formation of chains of particles in the Kob-Andersen (4:1) and Wahnström (1:1) model liquids on cooling and supercooling

V.A. Levashov¹

¹*Technological Design Institute of Scientific Instrument Engineering, 630055, Novosibirsk, Russia. E-mail: valentin.a.levashov@gmail.com*

Investigations of structural changes happening with liquids on cooling and supercooling continue to attract significant attention as there is still no sufficient understanding of the connection between the structural changes and the dynamic slowdown. Previously, liquids' structures were usually discussed from the local perspective. Thus, the environments of individual particles were classified and it was assumed that the changes in populations of these local or medium-range environments should be related to the changes in liquids' properties. Here, we report on the structural evolutions of the binary Kob-Andersen (KA) (4:1) and Wahnström (1:1) model liquids using a different approach. The approach is based on the previously not discussed observation that in the liquid and supercooled liquid states some particles form nearly linear chains in the temperature region where the crystallization process has not been observed. Depending on the chain definition, it is possible to speak about the chains containing more than 8 particles. The average number of chains monotonically increases as the temperature of the liquid decreases. We also found that the number of chains remains nearly constant in the inherent structures (IS) obtained from the parent structures (PS) above the potential energy landscape (PEL) crossover temperature (PELCT). Then, below the PELCT, the average number of chains in the IS increases, as the temperature of the PS decreases. Counter-intuitively, for the KA system, we found that below the PELCT the number of chains in the PS can be larger than the number of chains in the corresponding IS. This, in our view, indicates that in the supercooled liquid there is some delicate beyond medium-range order that is being destroyed by the relaxation procedure from the PS to IS. Calculations of the distributions of the potential energies (PE) of the particles in linear chains show that the particles forming the chains tend to have higher PE than the particles which are not in the linear chains. We also found that the particles forming the chains diffuse at a slightly lower rate than the particles that do not belong to the chains. Finally, we address the lifetimes of the observed chains, which happen to be smaller than the α -relaxation time of the system. In our discussions, we compare the results for the chains with the results obtained within the topological cluster classification approach.

INTRODUCTION

Search for a hidden ordering of particles in supercooled liquids (SCL), that may lead to understanding of the dynamic slow down at the glass transition, continues for decades [1–14]. Earlier studies were usually focused on considerations of local atomic environments of individual particles often limited by the nearest neighbor shells [1, 2, 15–18]. In more recent studies, it has been demonstrated that an order associated with the second and more distant neighbors (a medium-range order) is also important for understanding the liquids' dynamics and, in particular, the relevant relaxation timescales [4, 13, 18–31].

Numerical simulations (NS) represent an invaluable tool in the structural studies of liquids [1–8, 10–13, 16–21, 23–36]. There are several model systems which are actively used in NS of SCL. One of these is the Kob-Andersen (KA) binary system (KAS) consisting of 80% of larger *A*-particles and of 20% smaller *B*-particles [32, 33]. This model has been very extensively studied in a number of different contexts (see, for example, Ref. [18, 28, 32–43]). In particular, there were studies of the short and medium range order from the perspective of local environments of selected particles [4, 18, 28, 32–42]). Another

system that has been extensively studied previously is the binary equimolar Wahnström system (WS) [44, 45].

In this paper, we discuss a particular observation made on the KAS and WS. Thus, for the KAS, we found that on decrease of the temperature larger *A*-particles exhibit an increasing tendency to form approximately linear chains. In the WS the chains are formed by the smaller *B*-particles and also by all particles.

We note that the linear chains that we discuss, generally, are not related to the results concerning the chain-like cooperative motion extensively discussed previously [38].

In our view, the presented results are of significant interest as they explicitly demonstrate and partially elucidate the presence of an angular ordering on length scales exceeding 7 or 8 distances between the nearest neighbors. It is also possible that the chains of particles that we observe represent the precursors of the crystal nuclei.

We came to the observation of the linear chains in the KA system occasionally. Our initial goal was to perform for the KA system the investigation, which is similar to the one presented in our previous work [13] (despite the fact that a somewhat similar study has been performed before [42]). In the process of reviewing the related literature, in particular Ref.[18], we attempted to observe

arXiv:2209.07981v2 [cond-mat.soft] 10 Oct 2022

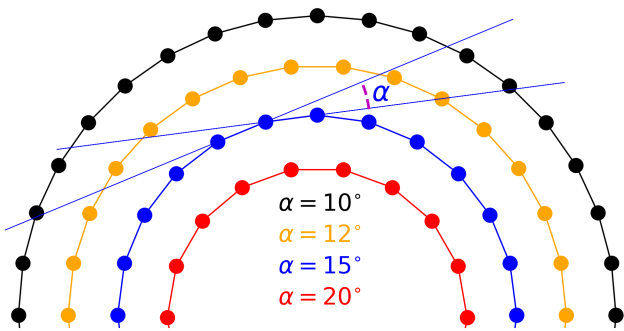


FIG. 1. For simplicity, we show the illustration for the definition of chains in $2D$. We study $3D$ systems. The shown blue chain of 13 particles corresponds to the chain $C(13, 15^\circ)$. It is the extreme case of the 15° chains because all angles between the nearest links in it are equal to 15° . For the chain of N particles to be counted as $C(N, \alpha_{max})$ all angles between the nearest links in the chain should be smaller than α_{max} . The lengths of all links in the shown chains are the same.

visually the “11A” (Ref.[18]) locally favored structure. Thus, we isolated the environments of a few selected B -particles up to the second neighbors and visually analyzed them. It became obvious from this analysis that it is possible to speak about the presence of nearly linear chains of large particles in the system. The related structure files in the “xyz” format are provided in the supplemental materials (SM).

The paper is organized as follows. In section , we briefly discuss the details of the simulation procedure and data analysis. More details are provided in the SM. In sections , we define the chains. Then, in section , we present the results concerning the numbers of chains in the parent liquid and the corresponding inherent structures. In this section, we also discuss the energies and the diffusion rate of the particles forming the chains, and the lifetimes of the chains. We conclude in section .

THE USED POTENTIAL AND SIMULATIONS DETAILS

In our simulations, we used the modified forms [46] of the Kob-Anderson potentials [32, 33]. The unmodified Kob-Anderson potentials are the shifted Lennard-Jones potentials with the parameters of length, σ_{ab} , and energy, ϵ_{ab} , chosen in a particular way. The modified potentials go to zero at the cutoff distances $r_{abc} = 2.5\sigma_{ab}$ with zero derivatives (forces). The same modified potentials have been used, for example, in Ref.[18, 34, 35, 46]. We provide more details on the used potentials and the simulation procedure in the supplemental materials (SM). Masses of all particles are assumed to be the same, m . The chosen units of length, energy and time are: $\sigma \equiv \sigma_{AA}$, $\epsilon = \epsilon_{AA}$, $\tau \equiv \sqrt{m\sigma^2/\epsilon}$.

We performed NVT simulations mostly on the (4:1)

Kob-Anderson system of 8000 particles (6400 A -particles and 1600 B -particles). The average density of the particles was $\rho_o = 1.2\sigma^{-3}$. We also performed some of the simulations on the system containing $64 \cdot 10^3$ particles.

We used the LAMMPS molecular dynamics (MD) program [47–49].

At every considered temperature we performed (10 for the systems of 8000 particles)/(6 for the system of $64 \cdot 10^3$ particles) simulations starting from independent structures. In each of these simulations, we accumulated (100 for the systems of 8000 particles)/(20 for the system of $64 \cdot 10^3$ particles) configurations. For $T > 0.46$, the mean square displacement (MSD), $\langle (\Delta r)^2 \rangle$, which corresponded to the time interval between the two consecutively saved structures was larger than 0.1 for the A -particles. For this reason, we believe that for $T > 0.46$ all saved structures can be considered as independent. Then, in the temperature interval $0.42 \leq T \leq 0.46$, the independence of the saved structures, obtained in the same simulation run, is questionable. For $T \leq 0.42$ it is reasonable to assume that the structures obtained in the same simulation run are not independent. In any case, at all studied temperatures, we analyzed all of the obtained structures, (1000 for the systems of 8000 particles)/(120 for the system of $64 \cdot 10^3$ particles), as independent.

The ISs were produced using the FIRE algorithm [50, 51] within the LAMMPS program Ref.[47–49]. More details can be found in the SM.

To address the generality of the results obtained on the KAS, we also studied the Wahnström system (WS) [44] of particles, as it is described in [41]. In these simulations, we used the shifted-force forms of the pair potentials [52]. The simulations for the WS were performed in the NVT ensemble for the system containing 8000 particles. The implemented relaxation procedure was similar to the one used for the KAS. At every studied temperature, we accumulated 100 structures of the parent liquid and produced from these parent structures (PS) 100 inherent structures (IS).

DEFINITION OF CHAINS

We say that there is a link or a bond between two large A -particles if the distance between them is smaller than the cutoff distance, r_{AAc} , corresponding to the position of the 1st minimum in the partial pair density function of AA particles, i.e., $r_{AAc} = 1.4\sigma$ (see the SM).

We say that N large A -particles form a $C(N, \alpha_{max})$ chain if all nearest links in the chain intersect at the angles $\alpha < \alpha_{max}$. See Fig.1,2.

In the SM, we describe the algorithm that has been used to find the chains in the system.

ANALYSIS OF THE OBTAINED DATA

Observation of the linear chains

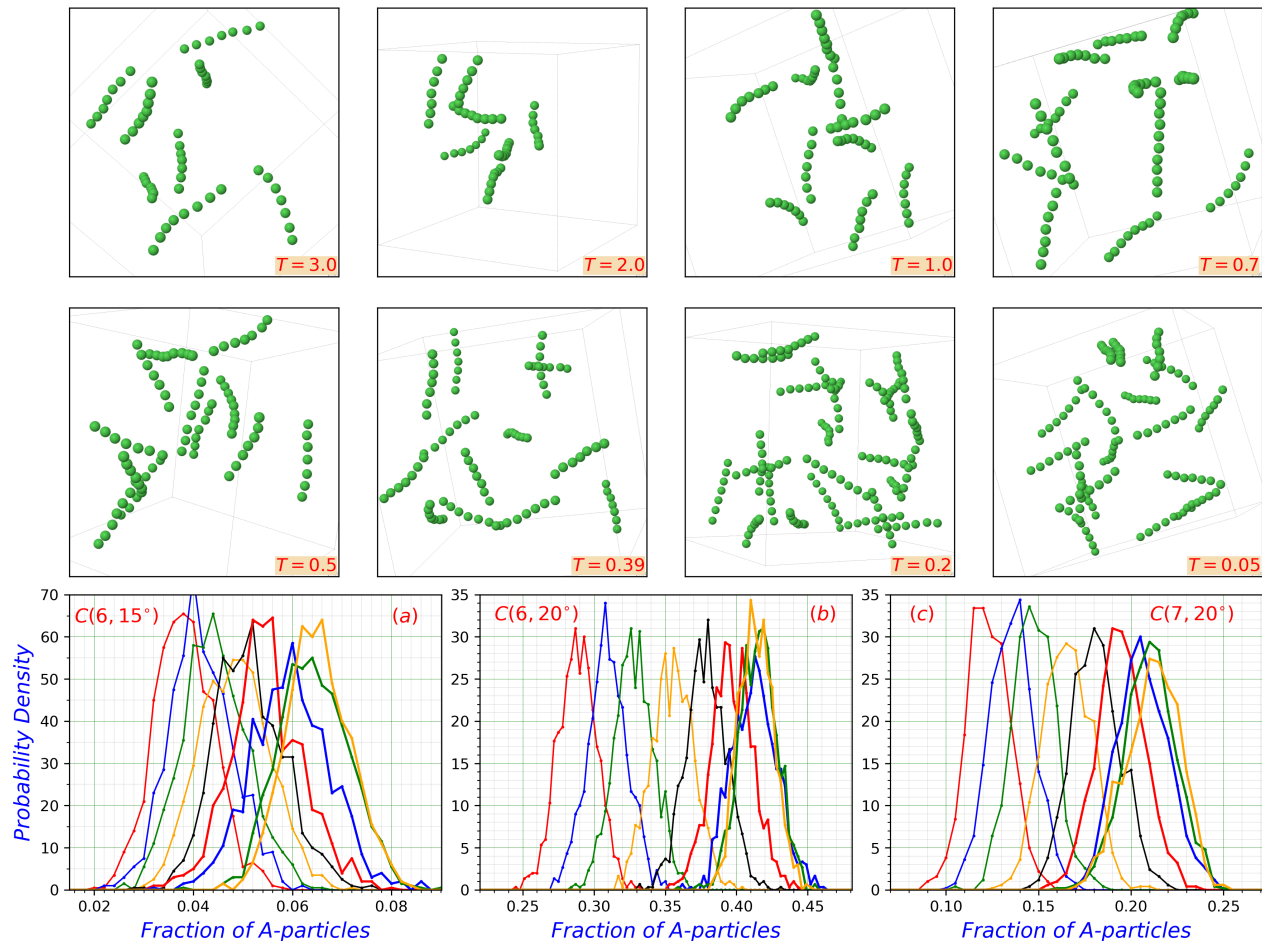


FIG. 2. In a particular configuration of particles, at a given temperature, there are A -particles that form approximately linear $C(7, 15^\circ)$ chains. In two upper rows, only such A -particles are shown. Different panels show the results from the selected configurations at selected temperatures. In the SM we provide several structure files, containing the coordinates of the A -particles forming the chains, that can be visually examined with practically any structure-view program. In the lower row, we show the probability distributions for the numbers of A -particles forming different chains at different temperatures. Panels (a), (b), and (c) correspond to the chains $C(6, 15^\circ)$, $C(6, 20^\circ)$, and $C(7, 20^\circ)$ correspondingly. The abscissa-axes in these plots show the fraction of A -particles participating in the chains relative to all A -particles in the system. Different curves – from the left to the right – correspond to the temperatures $T = 3.0, 2.0, 1.5, 1.0, 0.7, 0.5, 0.39, 0.20, 0.05$.

on the parent and inherent structures

The upper two rows in Fig. 2 show the snapshots of the $C(7, 15^\circ)$ A -particles-chains found in the 8000-particles system at selected temperatures. Only particles forming the chains are shown. It is clear that at lower temperatures there are more chains than at higher temperatures.

We note that it does not follow from the shown data that the chains at lower temperatures agglomerate into some more complex structures. However, more detailed visual examinations of the structures show, especially at temperatures below $T = 0.50$, that it is eventually possible to see several closely located chains which are approximately parallel to each other. Sometimes it is a longer chain and one or two shorter chains which are neigh-

bors that are approximately parallel to each other. Some of such arrangements can be seen in the structure files provided in the SM. This point is, in our view, of importance from the following perspective. Let us imagine that on cooling in the liquid start to form some precursors of crystal nuclei. Then, it is reasonable to expect that in such crystal-like precursors can be found somewhat aligned chains of the A -particles. However, at least at $T > 0.50$, we do not see often the closely positioned chains that are approximately aligned, i.e., most of the chains appear to be isolated. Thus, it is possible that the observed chains represent the 1D ordering and they are not a part of some more complex ordered structures. This issue requires further investigations, of course.

Panels (a,b,c) in the 3rd row of Fig. 2 show the proba-

bility distributions for the numbers of particles involved in all chains of a particular type in instantaneous configurations. As the temperature is reduced, the probability distributions shift to the right, i.e., the numbers of particles participating in the chains statistically increase. The data originate from 1000 instantaneous configurations of 8000 particles produced in 10 independent runs.

In Fig. 3, the red curves and the red solid circles show how the average numbers of particles in all chains of a particular type depend on the temperature.

In every panel there are three red curves that show the average value and the average value $\pm\sigma_{mean}$. We see that the average numbers of particles involved in the chains monotonically increase, as the temperature of the liquid decreases. The more abrupt rise in the numbers of chains in the temperature range $0.3 < T < 0.5$, in view of [10], might be related to the proximity of the temperatures at which the crystallization has been observed $T \sim 0.41 \pm 0.02$ [10]. The crystallization manifests itself, in the considered system, by the appearance of the regions containing FCC-crystals of A particles.

We do not discuss the process of crystallization here. The points that we make here are the following. First, we note that the observation of the development of the chain-like ordering is a new result. Second, in our view, the observed development of the linear ordering clearly shows that in the considered liquid there are orientational correlations extending beyond, at least, the 7th nearest neighbors (from one end of the chain to another end). Third, we suggest that the observed linear chains might represent the precursors of the crystal nuclei that may or may not realize.

The blue curves in Fig. 3 correspond to the results obtained on the inherent structures (ISs).

Practically, all shown blue curves exhibit an abrupt crossover at the potential energy landscape (PEL) crossover (PELC) temperature (PELCT). Originally, the PELCT was observed by consideration of the potential energies of the ISs [34]. As far as we know, there is still no clarity with respect to which structural changes in the liquid the PELC is related. Our results concerning the presence of the linear chains are purely geometrical. Therefore, it is reasonable to think that the formation of chains is closely related to the structural ordering that underlies the PELC. It is possible, of course, that the observed chains represent some parts of more complex structures. On the other hand, as follows from the subsection (), the numbers of several types of clusters are also sensitive to the PELC. Thus, there are many “geometrical objects” whose number is sensitive to the PELC.

Of particular interest is the relation between the red and blue curves corresponding to the chains $C(6, 15^\circ)$, $C(6, 20^\circ)$, $C(7, 15^\circ)$, $C(7, 20^\circ)$, $C(8, 15^\circ)$, $C(8, 20^\circ)$, and $C(9, 20^\circ)$. For these chains, in the supercooled liquid range of temperatures, $0.4 \lesssim T \lesssim 1.0$, we observe that the average number of chains in the ISs is smaller than the number of chains in the parent structures (PS). This is a counter-intuitive behavior. Indeed, since the ISs

are more relaxed than the PSs, it is natural to expect that there always should be more chains in the ISs. In our view, the obtained results suggest that in the parent supercooled liquid there develops some delicate, beyond medium-range, order that is destroyed by a “rough” relaxation procedure by which the ISs are produced from the PSs. The linear chains either represent this order or represent a part of this order. It is also possible that the decrease in the number of chains in the transition from the parent to inherent structures is related to the fact that the pressure of the inherent structures becomes negative at $T \approx 0.8$. The pressure of the inherent structures becomes even more negative as the temperature of the parent structures further decreases. See the SM and, for example, Ref.[53–55] in this context. We note that in Ref.[53] it has been shown that at $\rho_o = 1.2$, that we study in this paper, the inherent structures (under the negative pressure) remain globally homogeneous.

On the other hand, at temperatures above the PELCT the relaxation procedure increases the number of chains to some nearly constant value. Thus, even a “rough” relaxation can increase the number of chains in the system.

The results from the system of 64000 particles are also shown in Fig. 3 as open-green and open-cyan circles.

Results for the selected clusters obtained with the topological cluster classification (TCC) program

As shown in Fig.3, the temperature dependencies of the average numbers of particles (NoPs) involved in the chains calculated on the IS exhibits a crossover at the PELCT. While this result is of interest, it is necessary to note that this number is not the only structural parameter exhibiting the PELC.

To address this point, we used the topological cluster classification program and studied the temperature dependencies of the NoPs involved in the selected local clusters [18, 41, 45]. These temperature dependencies for the parent and inherent structures are shown in Fig. 4. It follows from the data that the PELC is observable for all studied clusters, while it is significant only for the 11A clusters. The case of 11A clusters is also of special interest because for these clusters the presence of the crossover is quite obvious even from the analysis of the parent structures. This is in agreement with Ref. [18] in which it has been suggested that 11A clusters play a special role in the dynamic slowdown.

We also statistically studied the overlap between the particles forming the chains and the particles forming the 11A clusters. We found that the overlap is essentially random.

Concerning the generality of the obtained results

To address the generality of the results obtained on the KAS we also studied the Wahnström system (WS)

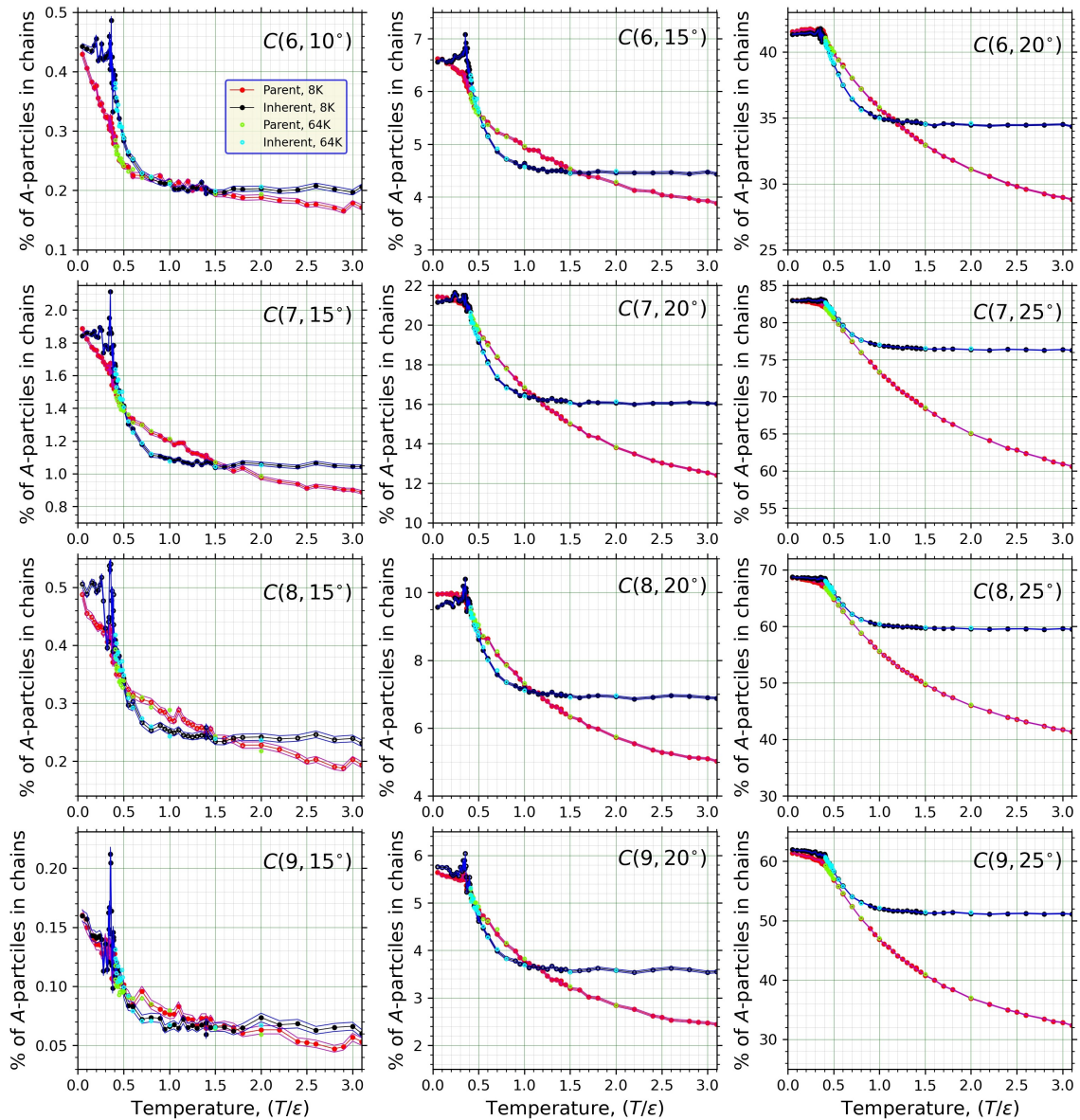


FIG. 3. The dependencies of the average percentage of A -particles in all chains of a particular type on the system's temperature. The percentage is with respect to the total number of A -particles in the system. The panels in the same row correspond to the chains with the same number of particles, but the limiting inclusion angles are different in different columns. The red solid circles connected by the red lines show the results from the parent structures obtained on the system of 8000 particles. There are the average curves and also the average curves plus/minus the sigma of the mean (magenta). The light green open circles correspond to the results obtained on the system of 64000 particles. The error bars are not shown. The black solid circles correspond to the results obtained on the inherent structures of the system of 8000 particles. The blue curves show the errors of the mean for the inherent structures. The cyan open circles correspond to the results obtained on the system of 64000 particles. These results from the systems of 8000 and 64000 particles were obtained from 1000 and 120 configurations correspondingly.

[41, 44] of particles. We found that the development of chains in the WS on cooling is also present. However, in the WS the chains are formed by the smaller, "B", and all particles. Some of the obtained results are shown in Fig. 5. We are planning to report more results obtained on the Wahnström system in a separate publication.

We also studied the formation of the chains in the KAS

on cooling at zero pressure—the chains of A -particles form in this system too.

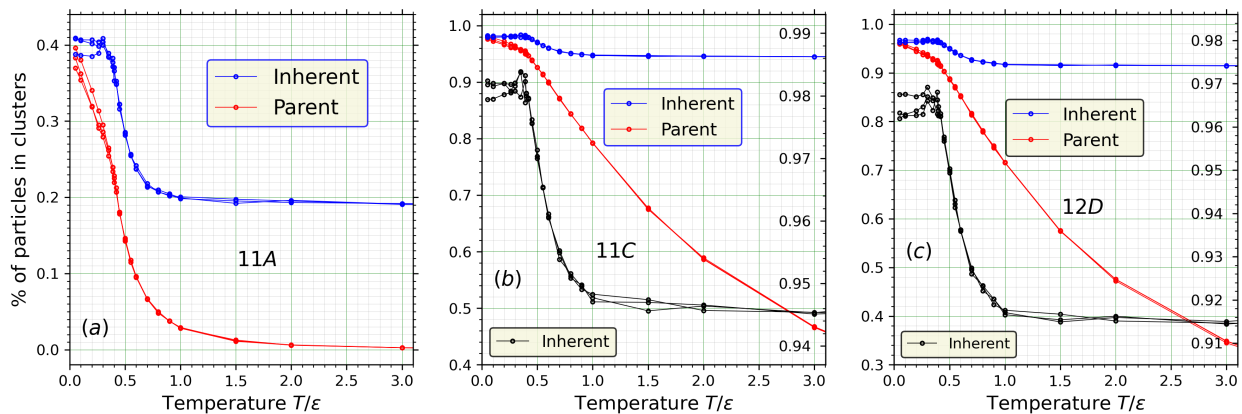


FIG. 4. The dependencies of the average percentage of both types of particles in the clusters of the selected types on the system's temperature. The percentage is with respect to the total number of particles in the system. The results from the inherent structures are also shown. In panels (b,c) the results from the inherent structures are also shown on different scales with the black curves. The scales corresponding to the black curves are shown on the right y -axes. The results have been obtained using the topological cluster classification analysis applied to the system containing 8000 particles. The results from three independent simulations are shown with three curves. 100 configurations were generated for data analysis in each simulation at each temperature.

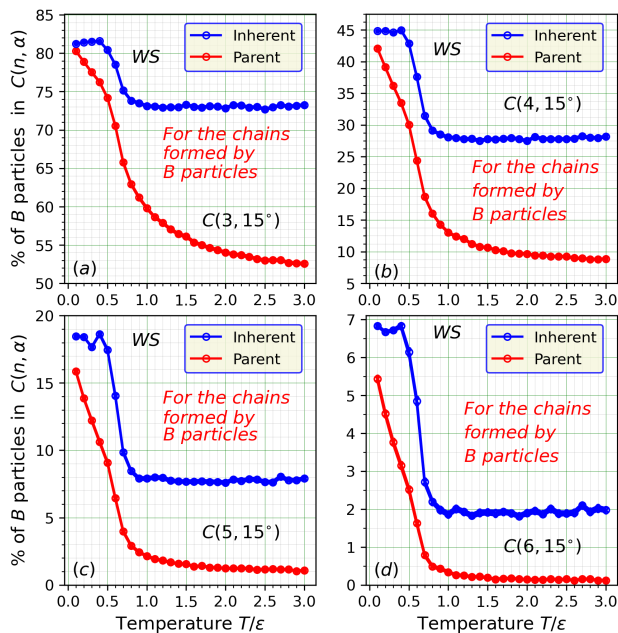


FIG. 5. The results presented in this figure are analogous to those in Fig.3(a,b,c,d,e,f). However, the shown data have been obtained on the Wahnström system (WS) of particles.

Distributions of the potential energies of particles forming the chains

It is of interest to compare the distributions of the potential energies (DoPE) of the A -particles participating in the chains with the DoPE of all A -particles. These results are shown in Fig.6(a,b,c). Another figure with

more data on the issue is provided in the SM. It follows from Fig.6(a,b,c) that the energies of the particles forming the chains are statistically higher than the energies of all A -particles. This result suggests that the chains do not represent the conformations of particles with the tendency to have a particularly high structural stability. It is also possible that the chains are located at the boundaries of some more stable structures. This issue requires further investigations.

In Fig.6(d) we show how the integrals of the squares of the differences between the curves, like those shown in panels (a,b,c) depend on the temperature. We see that these integrals start to grow as the temperature is reduced below the PELCT. This result also suggests the existence of the connection between the PELC and the chain formation.

Diffusion

Probably, the most basic question, which is of interest in the context of the observed chains, concerns the rate of diffusion of the particles that form the chains and how the rate of their diffusion compares to the rate of diffusion of other particles. In the context of the clusters of particles, for the Wahnström system, this question has been addressed in Fig.5(c) of Ref. [45]. Here, we follow the same approach for the KA system and compare the results for the chains with the results for the 11A clusters [18]. In panel (a) of Fig. 7 we show the time-dependencies of the mean square displacements (MSDs) of the particles that belong to the 11A and those that do not belong to the 11A clusters. As the temperature decreases, the differences between the curves corresponding to the same

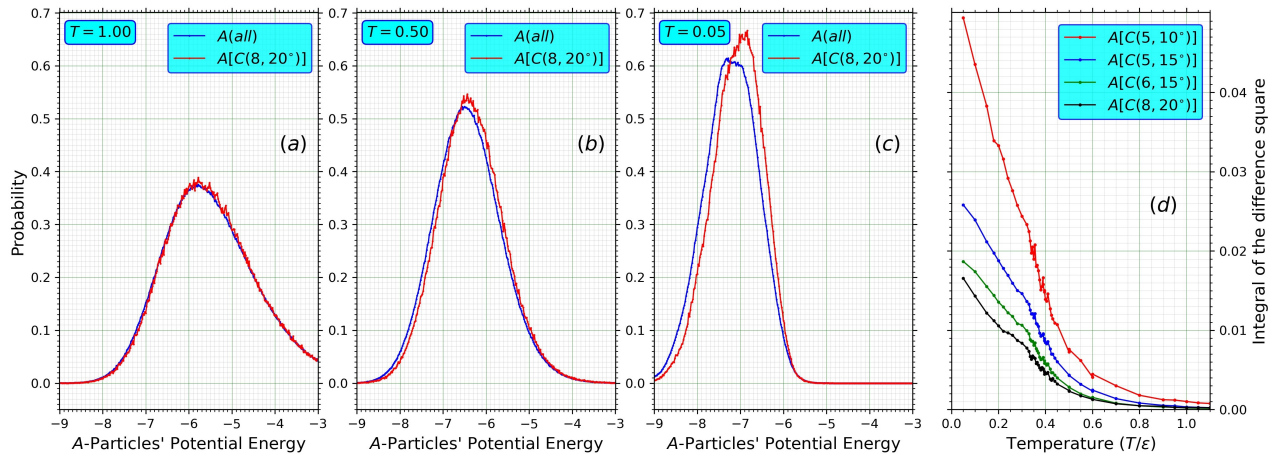


FIG. 6. The probability distributions (PDs) of the individual A -particles' potential energies for the $C(8, 20^\circ)$ chains at temperatures $T = 1.0$, $T = 0.50$, and $T = 0.05$ are shown in panels (a), (b), and (c) correspondingly. The red curves show the PDs of the A -particles belonging to the chains of a particular type. The blue curves show the PDs of all A -particles in the system. In panel (d) we show how the integrals of the squares of the differences between the red and blue curves depends on the temperature for the chains of different types.

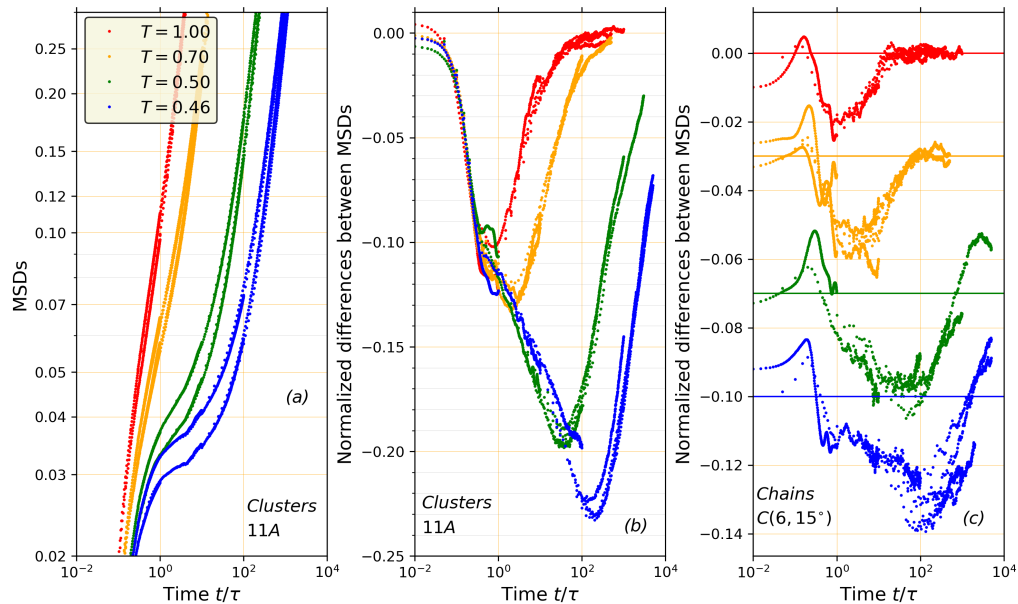


FIG. 7. (a) The two blue curves show the dependencies of the mean square displacements (MSDs) of the particles that belong to the 11A clusters and those that do not belong to the 11A clusters at $(T/\epsilon) = 0.46$. The particles that belong to the 11A clusters diffuse slower, i.e., to them corresponds the lower blue curve. The other curves in panel (a) show similar results at the other selected temperatures. If the results for the particles that belong and do not belong to the chains were plotted in panel (a) then they all, essentially, would coincide with the results for the particles that do not belong to the 11A clusters. For this reason, we do not show these data in panel (a). (b) In this panel, we plot the normalized differences between the MSDs for the particles that belong to the 11A clusters and the MSDs for the particles that do not belong to the 11A clusters. The normalization is to the MSDs of all particles, i.e., we plot $\{[MSD(in) - MSD(out)]/MSD(all)\}$. (c) The results shown in this panel are analogous to those in panel (b). However, these results are for the $C(6, 15^\circ)$ chains. The curves corresponding to the lower temperatures were displaced downwards. The horizontal lines of the same color as the data correspond to zeros for the displaced curves. Note that the “dynamic heterogeneity” effect for the $C(6, 15^\circ)$ chains is approximately five times smaller than the “dynamic heterogeneity” effect for the 11A clusters at all temperatures.

temperature increase. The differences are the largest at the late β -relaxation time, i.e., when the particles, on average, leave their cages. This behavior can also be observed in panel (b) that shows the normalized differences between the curves of the same color in panel (a). Notably, the difference-curves exhibit well-defined minimums that, as the temperature decreases, shift to the larger times, as expected. Note also that, at the lowest temperature, at the minimum, the normalized difference is approximately 23% of the MSD calculated by averaging over all particles. In panel (c), we show the results, analogous to those in panel (b), but for the particles that belong and do not belong to the $C(6, 15^\circ)$ chains. For the clarity of presentation, the results for the lower temperatures were shifted downwards. The comparison of the data in (c) with (b) shows that the slow-down effect for the particles in chains is approximately five times smaller than for the particles in 11A clusters. The smallness of the effect is the reason why we did not plot the MSDs corresponding to the chains in panel (a)– it would be difficult to distinguish between the chains-related curves. Nevertheless, panel (c) clearly shows that the slowdown-effect is there.

The data shown in Fig.7, for each temperature, were accumulated in several simulation runs of different lengths. The averaging was done over 1000 initial configurations in each run.

Lifetimes of the chains

It is also of interest to address the lifetimes of the chains (LoCs). Of course, the LoCs depend on the types of the chains. For example, the LoCs $C(7, 10^\circ)$ and $C(7, 20^\circ)$ should be different.

In the following, we define the chain-overlap correlation function (COCF) with the goal to address the chains' lifetimes.

We define $\mathcal{S}(N, \alpha, t)$ as the set of all A -particles in the system that participate in all $C(N, \alpha)$ chains at time t . Then, $\mathcal{N}(N, \alpha, t) \equiv \mathcal{N}(\mathcal{S}(N, \alpha, t))$ is the number of particles in the set $\mathcal{S}(N, \alpha, t)$. Further, $\bar{\mathcal{N}}(N, \alpha) \equiv \langle \mathcal{N}(N, \alpha, t) \rangle_t$ is the time-averaged number of particles in the chains $C(N, \alpha, t)$.

It is convenient to introduce the probability, $P(N, \alpha)$, for a randomly chosen particle to be in the set $\mathcal{S}(N, \alpha, t)$. Clearly, $P(N, \alpha) = \bar{\mathcal{N}}(N, \alpha)/N_A$, where N_A is the total number of A -particles in the system.

We define the overlap set, $\mathcal{O}_{(N_1, \alpha_1, t_1)}^{(N_2, \alpha_2, t_2)} \equiv \{\mathcal{S}(N_1, \alpha_1, t_1) \cap \mathcal{S}(N_2, \alpha_2, t_2)\}$, as the set of particles that simultaneously belong to the sets $\mathcal{S}(N_1, \alpha_1, t_1)$ and $\mathcal{S}(N_2, \alpha_2, t_2)$. Then, we define: $\mathcal{N}_{\mathcal{O}}^{(N_2, \alpha_2, t_2)}_{(N_1, \alpha_1, t_1)}$ as the number of particles in the set $\mathcal{O}_{(N_1, \alpha_1, t_1)}^{(N_2, \alpha_2, t_2)}$.

Finally, we define the average number of particles in the overlaps corresponding to configurations separated by time t : $\bar{\mathcal{N}}_{\mathcal{O}}^{(N_2, \alpha_2)}(t) \equiv \left\langle \mathcal{N}_{\mathcal{O}}^{(N_2, \alpha_2, t_o+t)}_{(N_1, \alpha_1, t_o)} \right\rangle_{t_o}$.

In further considerations, we assume that $N_2 \leq N_1$ and $\alpha_1 \leq \alpha_2$.

Let us consider two sets: $\mathcal{S}(N_1, \alpha_1, t_o)$ and $\mathcal{S}(N_2, \alpha_2, t_o + t)$. Since $N_2 \leq N_1$ and $\alpha_1 \leq \alpha_2$, all particles in the set $\mathcal{S}(N_1, \alpha_1, t_o)$ are also in the set $\mathcal{S}(N_2, \alpha_2, t_o)$. Therefore, at $t = 0$:

$$\bar{\mathcal{N}}_{\mathcal{O}}^{(N_2, \alpha_2)}(0) = \langle \mathcal{N}(N_1, \alpha_1, t_o) \rangle_{t_o} = N_A P(N_1, \alpha_1). \quad (1)$$

In the limit $t = \infty$, the “memory” of the initial configuration is gone. Therefore, any particle that at $t = 0$ was in the set $\mathcal{S}(N_1, \alpha_1, 0)$ has the same probability to be in the set $\mathcal{S}(N_2, \alpha_2, \infty)$ as any other particle in the system. Therefore:

$$\bar{\mathcal{N}}_{\mathcal{O}}^{(N_2, \alpha_2)}(\infty) = N_A P(N_1, \alpha_1) P(N_2, \alpha_2). \quad (2)$$

On the basis of (1,2) we define the chain overlap correlation function (COCF), as:

$$\mathcal{F}_{(N_1, \alpha_1)}^{(N_2, \alpha_2)}(t) \equiv \frac{\bar{\mathcal{N}}_{\mathcal{O}}^{(N_2, \alpha_2)}(t) - \bar{\mathcal{N}}_{\mathcal{O}}^{(N_2, \alpha_2)}(\infty)}{\bar{\mathcal{N}}_{\mathcal{O}}^{(N_2, \alpha_2)}(0) - \bar{\mathcal{N}}_{\mathcal{O}}^{(N_2, \alpha_2)}(\infty)}. \quad (3)$$

By definition, $\mathcal{F}_{(N_1, \alpha_1)}^{(N_2, \alpha_2)}(t)$ is equal to 1 (unity) at $t = 0$ and it is equal to zero at $t = \infty$.

We also can rewrite (3) using the probabilities:

$$\mathcal{F}_{(N_1, \alpha_1)}^{(N_2, \alpha_2)}(t) \equiv \frac{\frac{\bar{\mathcal{N}}_{\mathcal{O}}^{(N_2, \alpha_2)}(t)}{N_A P(N_1, \alpha_1)} - P(N_2, \alpha_2)}{1 - P(N_2, \alpha_2)}. \quad (4)$$

We define the characteristic lifetimes of the chains as the times at which the functions $\mathcal{F}_{(N_1, \alpha_1)}^{(N_2, \alpha_2)}(t)$ decay to some chosen values. Thus, t_{ce} is the time at which some COCF decays to the value of $1/e$ and $\tau_{c0.2}$ is the time at which the COCF decays to the value of 0.2.

In Fig.8(a) we show the dependencies on time of the intermediate self-scattering function for the large (“A”) particles at selected temperatures. In panels (b) we show the dependencies on time of the normalized number of particles in the overlap between the $C(6, 15^\circ, t_o)$ and $C(6, 20^\circ, t_o + t)$ sets of chains. Note that, according to (1,2), the shown ratio is equal to 1 at $t = 0$ and it saturates to $P(6, 20^\circ)$ as the time increases, as can be compared with the corresponding panel of Fig.2. In Fig.8(c) we show the COCF defined in (3,4). In this panel, the black circles mark the intersections of the COCF with the lines used to define the COCF decay times.

The result shown in Fig.8 have been obtained from several independent simulation runs. In these runs, to obtain the correlation functions at different times, the structures were saved for later analysis with different time intervals between the saved configurations. Thus, the total lengths of the simulations runs were also different (for the same number of the saved configurations). It follows from panels (b,c) that for $T < 0.5$ the COCF can significantly vary from a simulation to a simulation. In our view, the reason for this is the insufficient total

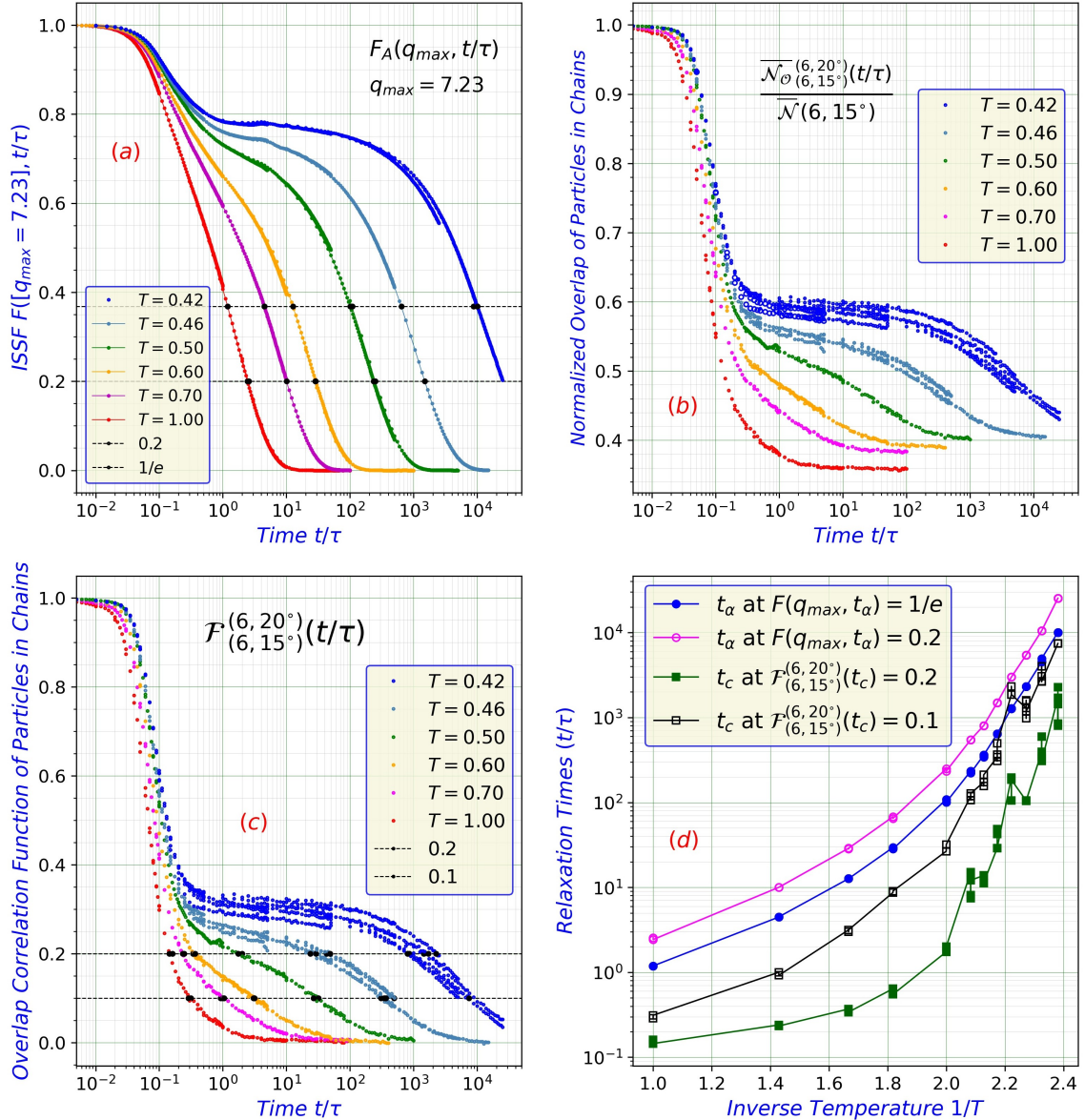


FIG. 8. (a) The dependencies of the intermediate self-scattering function of the A -particles on time at selected temperatures. The used value of the scattering wavevector, $q = 7.23$, corresponds to the position of the 1st maximum in the structure function (see the SM). (b,c) Address the lifetimes of the chains. (b) The dependencies on time of the ratio $[\overline{\mathcal{N}_\phi^{(6,20^\circ)}}(t/\tau)]/[\overline{\mathcal{N}}(6,15^\circ)]$. Note that this ratio is equal to 1 at $t = 0$ and, at large times, it saturates to a value that corresponds to the probability to find a randomly chosen particle in the set of $C(6,20^\circ)$ chains, as can be compared with Fig. 3. (c) The dependencies on time of the chain overlap correlation functions (COCF), $\mathcal{F}_{(N_1, \alpha_1)}^{(N_2, \alpha_2)}(t)$, defined in (3,4) at selected temperatures. The data in this panel were obtained by transformation of the data in panel (b). (d) The temperature dependencies of the relaxation times extracted from panels (a) and (c). The α -relaxations times extracted from (a) correspond to the times at which the intermediate self-scattering functions reach the values $(1/e) \approx 0.37$ (magenta open circles) and 0.2 (blue solid circles). The decay times of the (COCFs) correspond to the times at which the COCFs decay to the values of 0.2 (green solid squares) and 0.1 (black open squares). The lines are guides to the eye. The data in this figure have been accumulated in several sets of consecutive or independent simulation runs. In these runs the time intervals between the structures saved for later analysis were different. It can be seen from panels (b,c,d) that the results obtained for $T < 0.5$ can significantly vary from one simulation run to another. For this reason and since we did not perform careful statistical analysis of the data, the results for $T < 0.5$ should be considered as estimates.

duration of every particular simulation. Essentially, we observe that the relaxation is not homogeneous in time in the system of the studied size and for the considered time intervals. It is also possible that this behavior is related to some even slower relaxation processes (like ageing) that may proceed in the deeply supercooled liquids. The process of crystallization also can contribute to the observed behavior. However, we think that the process of crystallization can only contribute for the temperatures $T \leq 0.42$, i.e., only to the lowest temperature data shown in (b,c) [10]. Generally, the behavior at such low temperatures is not of interest for us here. Thus, while we show some data for $T < 0.46$, we are not particularly interested in their quantitative quality at present.

In Fig.8(d), we show the temperature dependencies of the relaxation times obtained from panels (a,c). As it can be expected, the relaxation times associated with the decay of the chains are shorter than the α -relaxation times, even though the $C(6, 20^\circ)$ chains do not represent a strict geometrical restriction. Indeed, approximately 40% of all A -particles participate in such chains at low temperatures.

An important comment concerns the significance of understanding and realization in the simulations of the infinite-time limit of the COCF (3,4). Indeed, in our considerations, we do not address the evolution of each chain individually. Instead, we always consider the total numbers of particles involved in the chains of particular types. For example, some particles can form a $C(N_1, \alpha_1)$ chain at t_1 . The same particles can also form the chains of the same type at t_2 . However, at some t , such that $t_1 < t < t_2$ the chain formed by these particles may not satisfy the required geometrical condition, i.e., it may not exist at t . Our approach does not address the time evolution of the chains in such a detailed way. However, the understanding and realization in simulations of the infinite time limit of the COCF justifies the use and physical meaning of the characteristic relaxation times extracted from the behavior of the COCFs.

CONCLUSION

In this paper, we reported about a structural property of the Kob-Andersen and Wahnström model liquids that has not been discussed previously. Thus, we have shown that in the Kob-Andersen system large A -particles exhibit a tendency for an approximately linear chain-like ordering which has been observed in the parent liquid structures above and below the potential energy landscape (PEL) crossover temperature. The observed chains can contain more than 8 particles. Thus, our results indicate that in the liquids there is beyond medium-range angular ordering. The observed chains can represent this ordering or be a part of a more complex ordering that requires further investigations.

The results obtained on the inherent structures show that the temperature dependence of the numbers of par-

ticles involved in the chains exhibits a marked crossover at the potential energy landscape crossover temperature. Since our definition of the chains is purely geometrical, it is possible that we found a structural feature that underlies or which is closely related to the phenomenon of the PEL crossover.

Besides, our results show that the relaxation procedures used to obtain the inherent structures can destroy the delicate ordering associated with the chain formation in the supercooled liquid range. It is also possible that the observed behavior is related to the fact that somewhat below the PEL crossover temperature the pressure of the system becomes negative and it becomes even more negative as the temperature of the parent structures further decreases.

In our view, it is natural to assume that the observed chains of particles should be related to the long-debated issue concerning the presence of crystallinity in liquids (see, for example, [12]). If the observed chains can be considered as crystallites, then the total number of particles participating in the chains characterizes the degree of crystallinity of the liquid. If this is so, then the increase in crystallinity that we observe, as the temperature decreases, shows that the liquid becomes more crystal-like at lower temperatures.

In this work, we, effectively, look at the one dimensional signature of the possible crystallinity of the studied liquid. In principle, it is possible that this crystallinity is just one dimensional. It is also possible, of course, to search for two dimensional signatures of crystallinity, i.e., to look for small plane-like regions.

We also investigated the rate of diffusion of the particles forming the chains and found that it is only slightly lower than the average rate of diffusion of all particles.

Then, we investigated the lifetimes of the observed chains. The obtained results show that there are several regimes in the decay of the chains which qualitatively resemble the decay regimes of the intermediates self-scattering function. However, the characteristic lifetimes of the chains are noticeably smaller than the α -relaxation times.

We also performed similar investigations on the Wahnström system of particles and the Kon-Andersen model at zero pressure. We found that the chains of particles form in those systems too. We are planning to report more detailed accounts of these results elsewhere.

In our view, further investigations related to the origin of the chain-like ordering are of significant interest.

ACKNOWLEDGEMENTS

We gratefully acknowledge access to the following computational resources: Supercomputing Center of Novosibirsk State University (<http://nusc.nsu.ru>).

Supplemental Materials for the Paper: Concerning the formation of chains of particles in the Kob-Andersen (4:1) and Wahnström (1:1) model liquids on cooling and supercooling

V.A. Levashov¹

¹*Technological Design Institute of Scientific Instrument Engineering,
630055, Novosibirsk, Russia. E-mail: valentin.a.levashov@gmail.com*

In these supplemental materials (SM), we describe the interaction potentials used in our simulations of the Kob-Andersen system (KAS) and provide the details of our simulation procedure. We also describe the algorithm used for the chain-search. Besides, for the reference, we show some of the standard well-known results obtained on the KAS. Finally, these SM contain the extended versions of some figures presented in the main text. Here, we focus on the KAS. The general scheme for obtaining the data on the Wahnström system (WS) was quite similar. We do not describe the details for the WS here.

I. ORGANIZATION OF THE SUPPLEMENTAL MATERIALS

In section II, we provide more details on the potential used in our simulations.

In section III, we describe in detail our simulation procedure.

In section IV, we describe the algorithm for the chain-search.

In section V, we show the pair distribution and the structure functions for the A -particles.

In section VI, we address the potential energies and pressures of the parent and inherent structures.

In section VII, we show the results for the means square displacement, diffusion coefficient, intermediate self-scattering function, and the α -relaxation time.

In section VIII, we compare our results for the diffusion coefficient with the earlier results.

In section IX, we provide more details concerning the distributions of the potential energies of the particles forming the chains.

II. THE USED POTENTIALS

In our simulations, we used the Kob-Andersen binary model system of particles [32, 33]. This system consists of 80% of larger A particles and 20% of smaller B particles. The masses, m , of all particles are the same. The particles interact via the pair potentials. These are the modified Lennard-Jones potentials [34, 35, 46, 56]. The modifications guarantee that the interactions between the pairs of particles of types a and b become zero at $2.5\sigma_{ab}$ [46]. The continuities of the derivatives of the potentials (the forces) at $2.5\sigma_{ab}$ are also guaranteed. The precise forms of the potentials are given by [35, 46]:

$$U_{ab}(r) = 4\epsilon_{ab} \left\{ \phi_{ab}^{LJ}(r) + \phi_{ab}^D(r) + C_{ab} \right\}, \quad (5)$$

where

$$\phi_{ab}^{LJ}(r) = \left(\frac{\sigma_{ab}}{r} \right)^{12} - \left(\frac{\sigma_{ab}}{r} \right)^6, \quad (6)$$

$$\phi_{ab}^D(r) = \left[6 \left(\frac{\sigma_{ab}}{r_{abc}} \right)^{12} - 3 \left(\frac{\sigma_{ab}}{r_{abc}} \right)^6 \right] \left(\frac{r}{r_{abc}} \right)^2, \quad (7)$$

$$C_{ab} = \left[7 \left(\frac{\sigma_{ab}}{r_{abc}} \right)^{12} - 4 \left(\frac{\sigma_{ab}}{r_{abc}} \right)^6 \right], \quad (8)$$

where $\phi_{ab}^{LJ}(r)$ (6) are the Lennard-Jones parts of the potentials. The terms $\phi_{ab}^D(r)$ (7) guarantee the continuities of the derivatives of the potentials at the cutoff distance $r = r_{abc} = 2.5\sigma_{ab}$. The constants C_{ab} (8) guarantee the continuities of the potentials at $r = r_{abc}$.

The length scales of the interactions between the particles of different types are: $\sigma_{AA} = \sigma = 1.0\sigma$, $\sigma_{BB} = 0.88\sigma$, and $\sigma_{AB} = 0.80\sigma$. Note that $\sigma_{AB} \neq (\sigma_{AA} + \sigma_{BB})/2 = 0.90$. Though, the difference between 0.88 and 0.90 is quite small. The energy scales are: $\epsilon_{AA} = \epsilon = 1.0\epsilon$, $\epsilon_{BB} = 0.5\epsilon$, and $\epsilon_{AB} = 1.5\epsilon$. The units of length and energy/temperature are σ and ϵ . The unit of pressure is ϵ/σ^3 . The unit of time is $\tau = \sqrt{m\sigma^2/\epsilon}$. We note that in Ref. [32, 33] a rescaled (a smaller) unit of time has been used $\tau_{KA} = (1/\sqrt{48})\tau$. On the other hand, the unit of time used, for example, in Ref. [34, 35, 56] is the same as the one used in our work.

III. DETAILS OF THE SIMULATION PROCEDURE

In our simulations we used the NVT ensemble within the LAMMPS program [47–49]. The very initial structure, from which we started all simulations, was the simple cubic lattice with the average density of all particles $\rho_0 = 1.2$. In this lattice, 4 planes of A particles alternated with 1 plane of B particles. Then, we “melted” this artificially created lattice within LAMMPS at temperature $T = 7.0$. At this high temperature the particles

T	dt	Δt	$\langle [\Delta r_A(\Delta t)]^2 \rangle, \langle [\Delta r_B(\Delta t)]^2 \rangle$	τ_α
6.0	0.0005 τ	10 τ	$\approx 12.1\sigma^2, \approx 17.3\sigma^2$	no data
5.0	0.0010 τ	20 τ	$\approx 20.4\sigma^2, \approx 28.1\sigma^2$	no data
4.0	0.0010 τ	10 τ	$\approx 7.7\sigma^2, \approx 11.0\sigma^2$	no data
3.0	0.0010 τ	20 τ	$\approx 15.6\sigma^2, \approx 21.5\sigma^2$	$\approx 0.23\tau$
2.5	0.0010 τ	20 τ	$\approx 8.2\sigma^2, \approx 12.1\sigma^2$	$\approx 0.28\tau$
2.0	0.0010 τ	20 τ	$\approx 5.7\sigma^2, \approx 8.5\sigma^2$	$\approx 0.36\tau$
1.6	0.0010 τ	20 τ	$\approx 3.9\sigma^2, \approx 6.2\sigma^2$	$\approx 0.49\tau$
1.5	0.0010 τ	30 τ	$\approx 5.2\sigma^2, \approx 8.1\sigma^2$	no data
1.4	0.0010 τ	50 τ	$\approx 7.6\sigma^2, \approx 11.1\sigma^2$	no data
1.2	0.0010 τ	50 τ	$\approx 5.5\sigma^2, \approx 8.3\sigma^2$	$\approx 0.80\tau$
1.0	0.0020 τ	100 τ	$\approx 6.8\sigma^2, \approx 10.8\sigma^2$	$\approx 1.19\tau$
0.8	0.0020 τ	100 τ	$\approx 3.4\sigma^2, \approx 5.8\sigma^2$	$\approx 2.39\tau$
0.7	0.0030 τ	150 τ	$\approx 3.0\sigma^2, \approx 5.2\sigma^2$	$\approx 4.49\tau$
0.6	0.0030 τ	150 τ	$\approx 3.0\sigma^2, \approx 5.2\sigma^2$	$\approx 12.7\tau$
0.55	0.0030 τ	300 τ	$\approx 1.25\sigma^2, \approx 2.43\sigma^2$	$\approx 28.3\tau$
0.50	0.0030 τ	300 τ	$\approx 0.37\sigma^2, \approx 0.94\sigma^2$	$\approx 100.7\tau$
0.48	0.0050 τ	500 τ	no data	$\approx 222.0\tau$
0.47	0.0050 τ	500 τ	no data	$\approx 360.8\tau$
0.46	0.0050 τ	500 τ	$\approx 0.22\sigma^2, \approx 0.63\sigma^2$	$\approx 642\tau$
0.45	0.0050 τ	500 τ	$\approx 0.137\sigma^2, \approx 0.41\sigma^2$	$\approx 1'265\tau$
0.44	0.0050 τ	500 τ	$\approx 0.122\sigma^2, \approx 0.35\sigma^2$	$\approx 2'313\tau$
0.43	0.0050 τ	500 τ	$\approx 0.078\sigma^2, \approx 0.24\sigma^2$	$\approx 4'945\tau$
0.42	0.0050 τ	500 τ	$\approx 0.0514\sigma^2, \approx 0.15\sigma^2$	$\approx 10'065\tau$
0.41	0.0050 τ	500 τ	$\approx 0.044\sigma^2, \approx 0.112\sigma^2$	N/D
0.40	0.0050 τ	500 τ	$\approx 0.035\sigma^2, \approx 0.094\sigma^2$	N/D
0.39	0.0050 τ	500 τ	$\approx 0.029\sigma^2, \approx 0.068\sigma^2$	N/D
0.38	0.0050 τ	500 τ	$\approx 0.028\sigma^2, \approx 0.071\sigma^2$	N/D
0.37	0.0050 τ	500 τ	$\approx 0.025\sigma^2, \approx 0.045\sigma^2$	N/D

TABLE I. The purpose of the table is to provide some technical details of the simulation procedure. Thus, the 1st column shows some temperatures at which the simulations have been performed. The 2nd column shows the values of the time step used at corresponding temperatures. To calculate the numbers of chains in the structures we generated 1000 configurations of 8000 particles in 10 independent runs at each studied temperature. Thus, in each independent run, we generated 100 configurations. The time interval between two consecutive structures, saved for later analysis, is provided in the 3rd column. In the 4th column, we show the mean square particles' displacements corresponding to the time between the two consecutively saved structures. Note that for temperatures $T \geq 0.55\epsilon$ the time interval between two consecutively saved structures is such that the mean square displacement of A -particles during this time interval is larger than σ^2 . Thus, it is natural to consider such structures as quite different. For such temperatures, this time interval is also significantly larger than the α -relaxation time. For the temperatures in the interval $0.46 \leq T \leq 0.47$ the dynamics is already quite slow and at these temperatures the MSDs corresponding to the time intervals between the two consecutively saved structures are smaller than σ . However, the time intervals between the two consecutively saved structures are still larger than than the corresponding α -relaxation times that we show in the 5th column. For temperatures $T \leq 0.46$ the α -relaxation time becomes quite large. Thus, for such low temperatures we did not aim to produce truly independent configurations. Instead, our purpose was to investigate how further structural relaxation affects the quantity of chains, even though it is clear that we do not study the truly equilibrium and truly independent configurations. Actually, precisely for this reason, we, starting from the very high temperatures, utilized 10 independent simulation runs. In any case, for $T < 0.46$ we adopted the following relaxation procedure. After reducing the temperature of the system from the temperature just above, we relaxed the system for $t = 50'000\tau$. After this relaxation, we collected 100 configurations during the same time $t = 50'000\tau$. The final configuration of the particles, after the data collection run, was used as the starting configuration for the next lower temperature. This was done for each of the 10 independent runs. In this way, we reduced the temperature down to $T = 0.05\epsilon$. For the larger system of 64'000 particles we followed the same procedure for those temperatures that we studied.

are mobile and it does not take much time to achieve the mean square displacement of particles corresponding to dozens of interatomic distances. We performed several of such initial consecutive equilibration runs. Then, still at $T = 7.0$, we performed several consecutive runs in

which the final structures for the restart files were separated from each other by time intervals corresponding to the MSDs corresponding to several dozens of interatomic distances. Thus, we assume that we produced several sufficiently different structures at $T = 7.0$. For the system

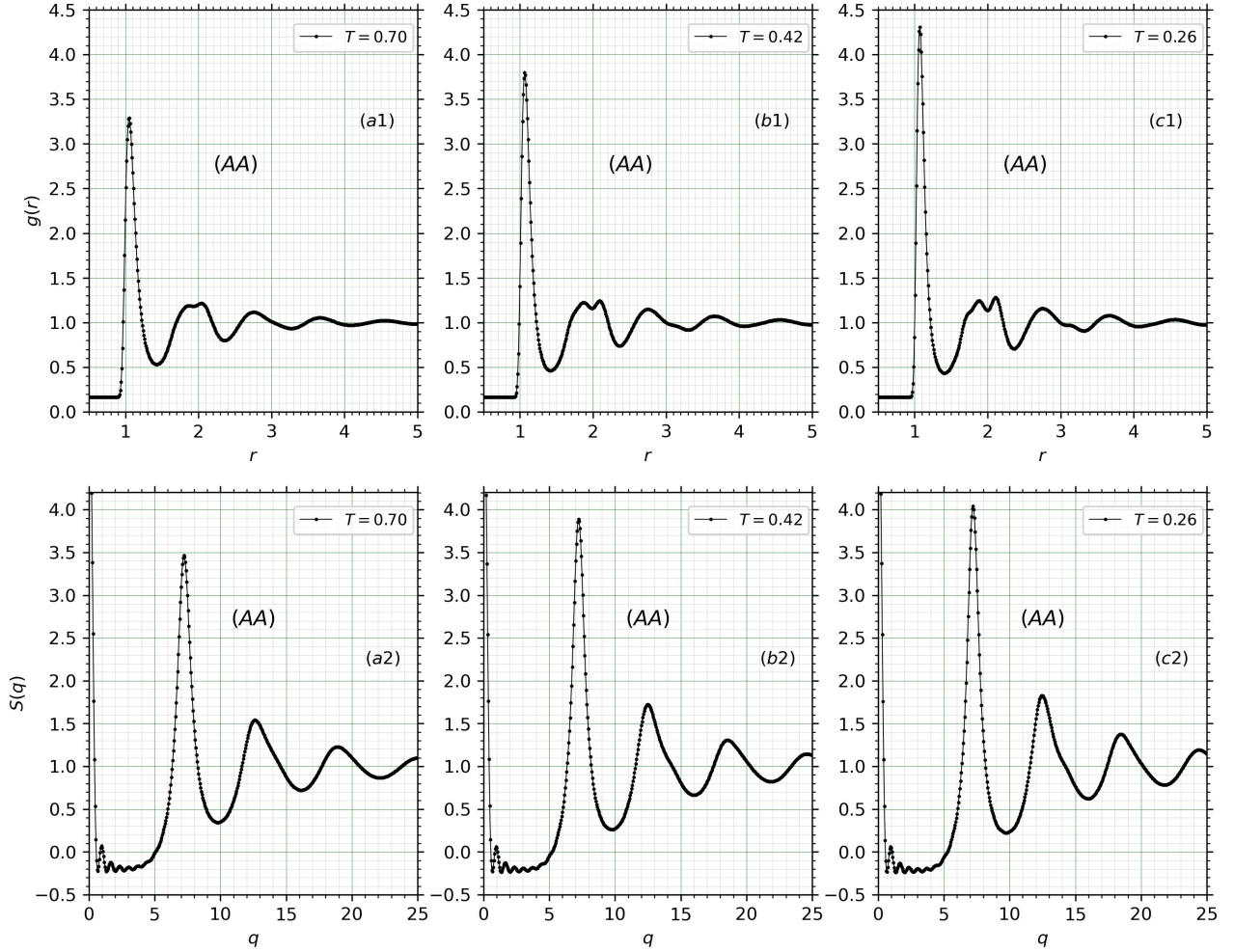


FIG. 9. Panels (a1), (b1), (c1) show the partial pair density functions, $g_{AA}(r)$, between the (AA) particles at temperatures $T = 0.70$, $T = 0.42$, and $T = 0.26$. These figures can be compared, for example, with the results shown in Fig.9 of Ref. [32]. Panels (a2), (b2), (c2) show the partial normalized structure functions $S_{AA}(q)$ obtained from the shown partial PDFs via the Fourier transform (11, 13). In our calculations, $R_{max} \approx 9.41$, i.e., the half-length of the edge of the cubic simulation box. Note that the 1st maximum in $S(q)$ occurs at $q \cong 7.2$.

of 8000 particles, we produced 10 structurally different restart files, while, for the system of 64000 particles, we produced 6 independent restart files for further use.

Then, concerning the systems of 8000 particles, for each of the created 10 configurations, we abruptly decreased the temperature to $T = 6.0$. Then, each of these 10 configurations was equilibrated, at $T = 6.0$, for the time corresponding to the mean average displacement of particles equal to approximately 25 interatomic distances ($t \approx 500\tau$), where $\tau = \sqrt{m\sigma^2/\epsilon}$. The used value of the time step was $dt = 0.0005\tau$. Then, starting from 10 structures equilibrated at $T = 6.0$, we generated 100 configurations for each of the initially equilibrated structures. Below, we address the time intervals between the saved structures in details. Thus, in total, we had 1000 configurations for the analysis. Further, the procedure described above for $T = 6.0$ was used to obtain the

structures at lower temperatures. The transition to a lower temperature was performed by reducing the temperature from the available previous higher temperature just above.

This procedure allows to achieve a further configurational divergence of the structures obtained from the 10 initial independent structures at $T = 7.0$ (in practice, it does not matter because these initial 10 structures at $T = 7.0$ are already very different). For the temperatures $T > 1.0$, the diffusion process is fast – the particles leave their cages within times $t < 0.5\tau$. Thus, for $T > 1.0$, it is not difficult to produce the equilibrated systems and then to produce the particles' configurations “separated” by mean particle displacement of several σ , i.e., presumably, quite different configurations. Note, the displacement of several σ guarantees that the “separation” time is larger than the α -relaxation time, as also

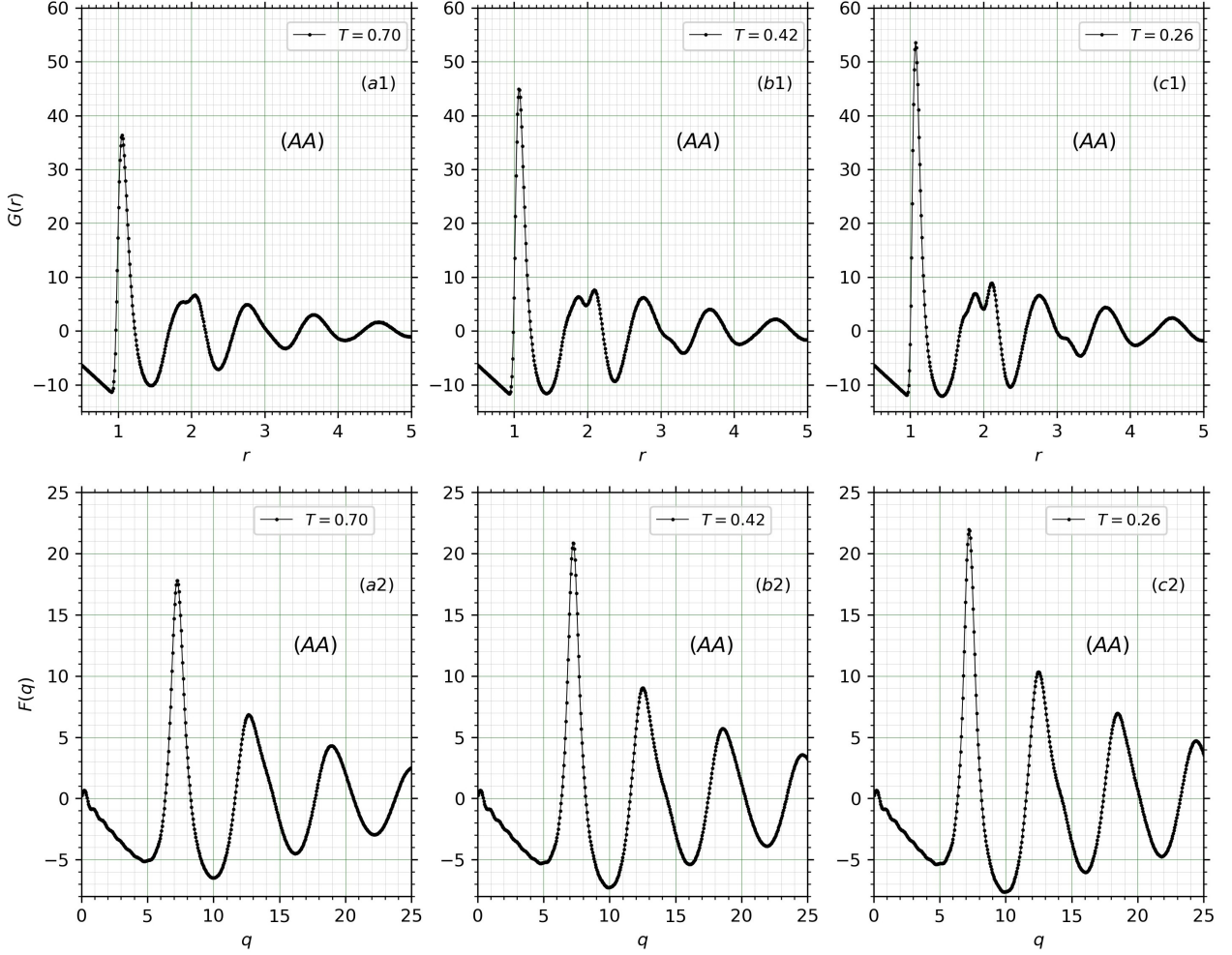


FIG. 10. Panels (a1), (b1), (c1) show the partial pair distribution functions (PDFs) between the (AA) particles at temperatures $T = 0.70$, $T = 0.42$, and $T = 0.26$. These figures can be compared, for example, with the results shown in Fig.9 of Ref. [32]. Panels (a2), (b2), (c2) show the intermediate self-scattering function $F_{AA}(q)$ obtained from the shown PDFs via the Fourier transform (11). In our calculations, $R_{max} \approx 9.41$, i.e., the half-length of the edge of the cubic simulation box. Then, $g_{AA}(r)$ is given by (9) and $G_{AA}(r)$ is given by (10). The inverse Fourier transform is given by (12). Finally, the connection between $F_{AA}(q)$ and $S_{AA}(q)$ is given by (13). Note that the 1st maximum in $F_{AA}(q)$ occurs at $q \cong 7.2$.

follows from Fig. 13 below. In the temperature interval, between $T = 5.0$ and $T = 1.0$ the used value of the time step was $dt = 0.001\tau$. In the temperature interval between $T = 1.0$ and $T = 0.5$ we increased the time step from $dt = 0.001\tau$ to $dt = 0.005\tau$. For $T \leq 0.5$ the time step was $dt = 0.005$. Further information, concerning the details of the simulation procedure, we provide in Table I and its description.

IV. ALGORITHM FOR THE CHAIN-SEARCH

In general, we say that (all different) particles $A_1, A_2, A_3, A_4, \dots, A_n$ form a chain if A_2 is in the list of the 1-st nearest neighbors of A_1 . Then, if A_3 is in the list of the 1-st nearest neighbors of A_2 . Then, if A_4

is in the list of the 1-st nearest neighbors of A_3 and so on. In addition, the angles $\angle(A_1A_2A_3), \angle(A_2A_3A_4), \dots, \angle(A_{n-2}A_{n-1}A_n)$ should all be sufficiently close to 180° .

To find the chains of A-particles, we used the following algorithm:

- 1) In the most external cycle (zero-order cycle) over all particles in the system we chose a particle "A" and label it as A_o .
- 2) Determine nearest neighbors of A_o according to the cutoff distance (1-st minimum in the AA-partial PDF). It is convenient, in a preliminary analysis, to determine the lists of neighbors for all A-particles.
- 3) Run the 1st internal order cycle over the neighbors of a chosen A_o .
- 4) A particular chosen A-neighbor of A_o we label as A_1 .
- 5) For the chosen A_o and A_1 we run again the cycle over

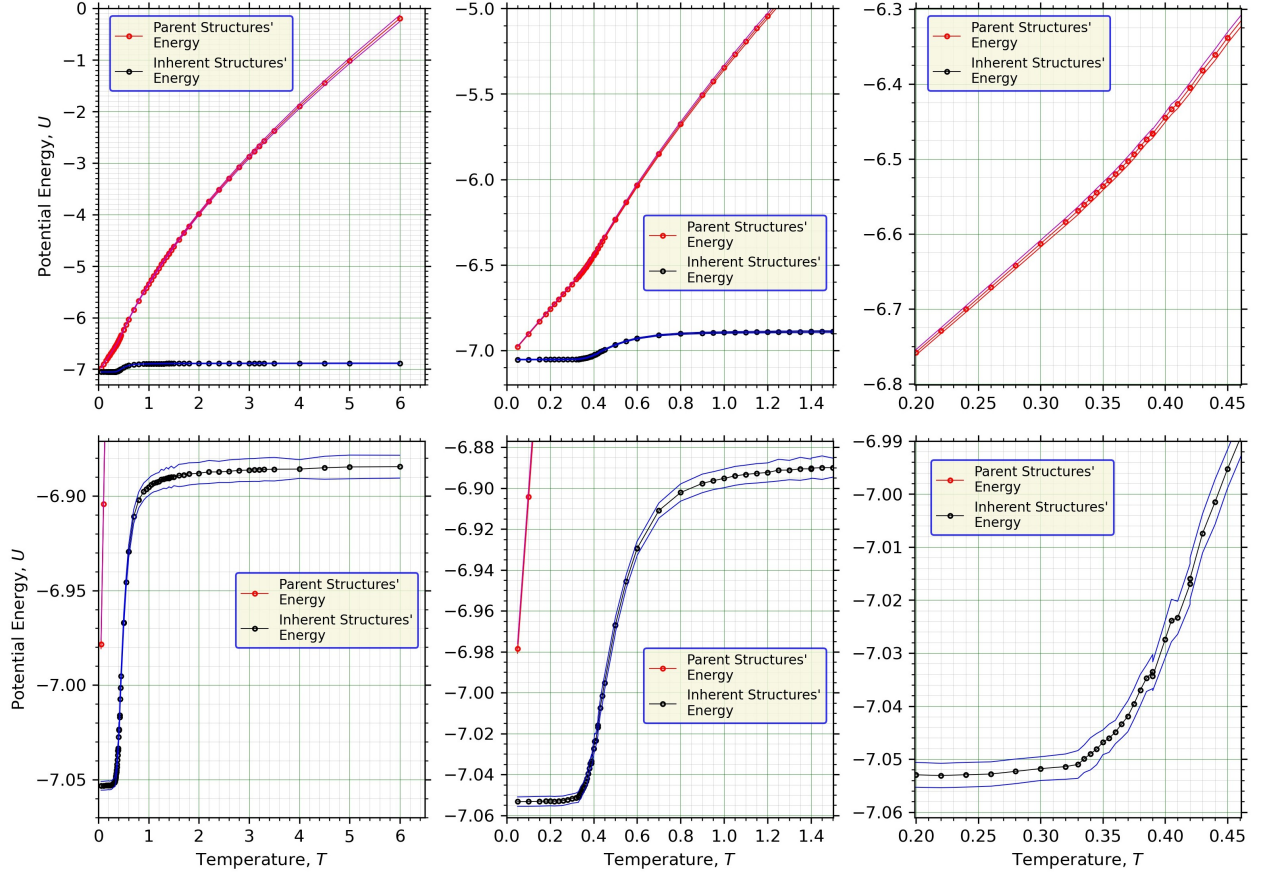


FIG. 11. Different panels show the same data on different scales. In all panels, the red curves show how the total average potential energy of the system per particle depends on the temperature. In every panel there are 3 red curves—the average and the average $\pm\sigma$, where $\sigma = \sigma(T)$ is the width of the distribution of the potential energies of individual structures (it is not the σ of the mean). The black curves in all panels show the temperature dependence of the average inherent structures' potential energy. The blue curves correspond to the black curves $\pm\sigma$ of the distribution of the inherent energy values of the individual structures (it is not the σ of the mean).

the neighbors of A_o (2nd order internal cycle). Another (different from A_1) particular chosen A -neighbor of A_o we label as A_2 .

6) For the selected A_o , A_1 , and A_2 , we check the value of the angle $\angle(A_1A_oA_2)$. If this angle is sufficiently close to 180° , according to a chosen angular cutoff, we say that there is a chain of the 3rd order.

7) If we are interested in chains of the 4th order, then the particle A_1 is used as the particle A_o previously. In particular, then there is a cycle over the 1st neighbors of A_1 (label them as A_3) and we check the angles $\angle(A_oA_1A_3)$.

8) If we are interested in the chains of 5th order, then, after the step 7) of this algorithm is completed, the particle A_2 is used as the particle A_o previously.

In particular, then there is a cycle over the 1-st neighbors of A_2 (label them as A_4) and the angle $\angle(A_oA_2A_4)$ is checked for the angle-cutoff condition.

9) If we are interested in the chains of higher order then we introduce more cycles over the neighbors of the particles at the ends of already determined chains of lower

order.

In principle, one can use a different and, probably, a slightly simpler algorithm to search for the chains of particles. Thus, it can be assumed that initially chosen particle, let say A_1 , is at one end of a chain. Then, assume that one of its 1st neighbor is A_2 . Then, let assume that A_3 is one of the 1st neighbors of A_2 . If the angle $\angle(A_1A_2A_3)$ is close enough to 180° then we say that these three particles form a chain of order 3. Then, if A_4 is the 1st neighbor of A_3 and the $\angle(A_2A_3A_4)$ is also close enough to 180° , then we have a chain of order 4 composed of particles (A_1, A_2, A_3, A_4) .

V. PAIR DISTRIBUTION FUNCTION AND INTERMEDIATE SELF-SCATTERING FUNCTION

In Fig.9, we show the normalized partial pair density functions, $g_{AA}(r)$ (9), between the A particles and the

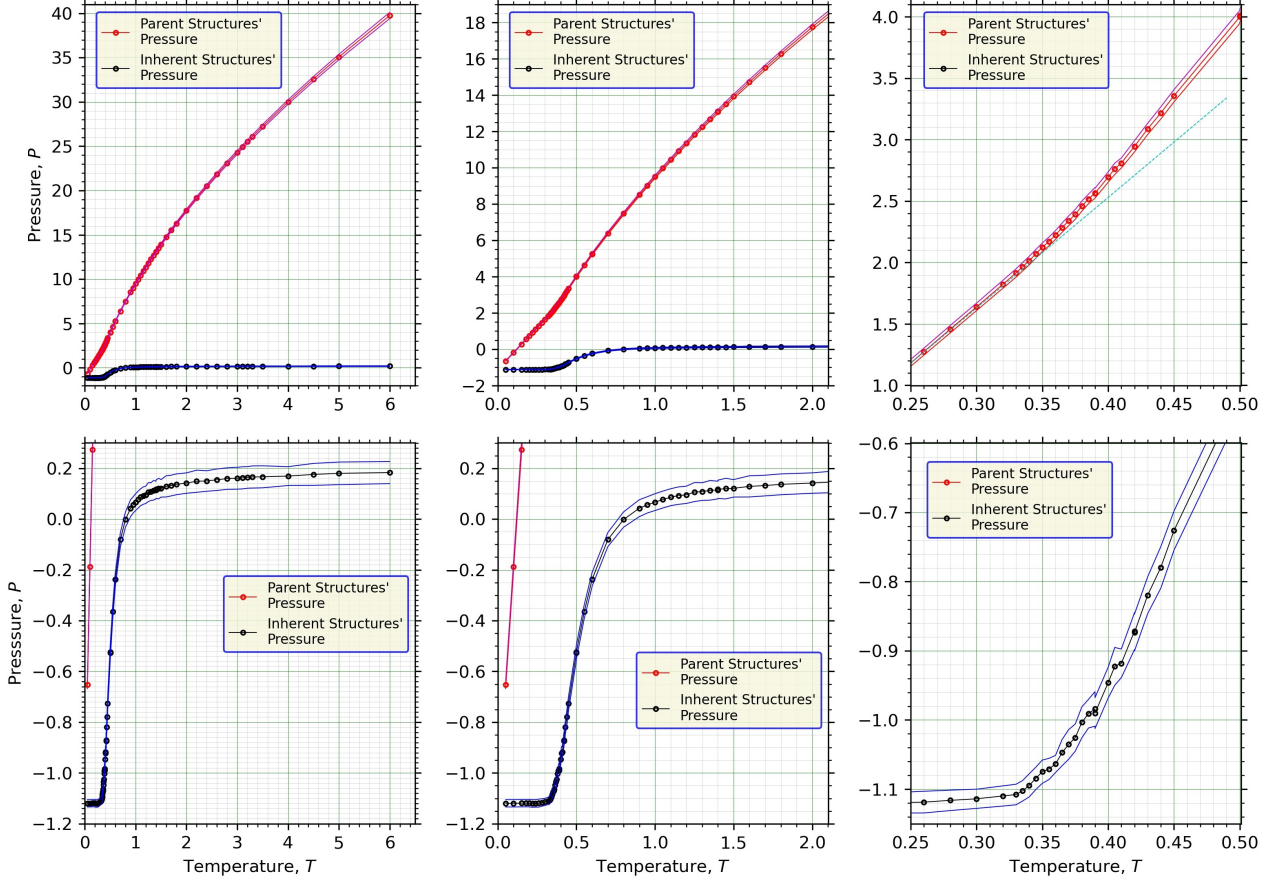


FIG. 12. Different panels show the same data on different scales. In all panels, the red curves show how the average pressure of the parent systems depends on the temperature. In fact, in every panel there are 3 red curves—the average and the average $\pm\sigma$, where $\sigma = \sigma(T)$ is the width of the pressure distribution of the individual structure (it is not the σ of the mean). The black curves in all panels show the temperature dependence of the inherent structures' average pressures. The blue curves correspond to the black curves $\pm\sigma$ of the distribution of the energy values from the individual structures (it is not the σ of the mean).

corresponding normalized partial scattering intensities, $S_{AA}(q)$ (9, 10, 11, 13), at selected temperatures. The results presented in these figures can be compared, for example, with the results shown in Fig. 9 of Ref. [32].

In Fig. 10, we show the functions which are closely related to $g_{AA}(r)$ and $S_{AA}(q)$, i.e., the partial pair distribution functions (10) and the partial intermediate self-scattering functions (11) for the AA -particles. The relations between the quantities presented in Fig. 10 and Fig. 9 are the following.

The normalized partial radial pair density between the A -particles is defined as:

$$g_{AA}(r) = \frac{\rho_{AA}(r)}{\rho_{oA}}, \quad (9)$$

where $\rho_{AA}(r)$ is the partial pair radial density between the A particles and ρ_{oA} is the average density of the A particles.

The partial pair distribution function for the A -

particles is defined as:

$$G_{AA}(r) = 4\pi\rho_{oA}r [g_{AA}(r) - 1]. \quad (10)$$

Then:

$$F_{AA}(q) = \int_0^{R_{max}} G_{AA}(r) \sin(qr) dr, \quad (11)$$

$$G_{AA}(r) = \frac{2}{\pi} \int_0^{Q_{max}} F_{AA}(q) \sin(qr) dq, \quad (12)$$

where the partial intermediate self-scattering function, $F_{AA}(q)$, is related to the to the partial normalized structure factor for the AA -particles according to:

$$F_{AA}(q) = q [S_{AA}(q) - 1]. \quad (13)$$

The limit of integration R_{max} in (11), in our case, is the half of the edge-length of the cubic simulation box.

The behavior of the functions presented in Fig. 9, 10, is well known. It is worth to note only that the position

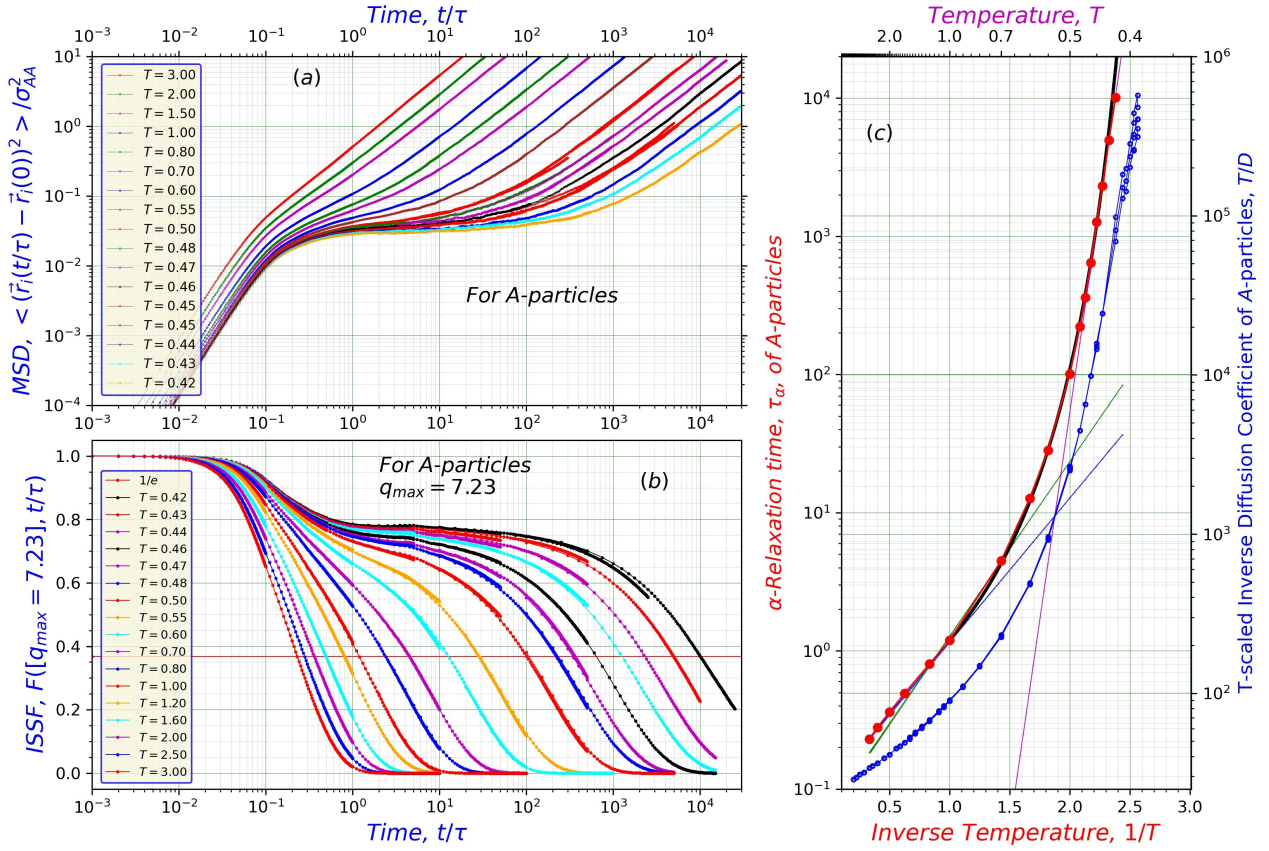


FIG. 13. Panel (a) shows the dependencies of the mean square particles' displacements (MSDs) on time for selected temperatures. The results have been obtained on the system of 64'000 particles to reduce fluctuations of the results at large times at low temperatures. For some temperatures, several sets of runs have been performed. The MSDs at the largest available times were used to produce the blue curve in panel (c). Panel (b) shows the dependencies of the intermediate self-scattering functions (ISSFs) on time for selected temperatures. The data have been obtained on the system of 8'000 particles. For some temperatures, several sets of consecutive runs have been performed. The slow relaxation that is present in the system at low temperatures, $T < 0.46$, is likely to cause the difference between the results from these runs. In general, at 1st, we run the longest simulation with the largest time-interval between the saved configurations. These configurations were used to calculate the ISSF at the largest times. The restart file after this the longest run was then used in a shorter run with a smaller time interval between the saved configurations. The configurations from this shorter run were used to calculate the ISSF at smaller times. The α -relaxation times, τ_α , were defined/determined as the times at which the ISSFs decay to the value $1/e$, which is shown with the horizontal pink line. Panel (c) shows the temperature dependencies of the α -relaxation time, τ_α , and the temperature-scaled inverse diffusion coefficient, T/D . Several fits to the data are shown with the line segments and discussed in the text.

of the 1st maximum and minimum in $g_{AA}(r)$ occur at $r_{max} \approx 1.05$ and $r_{min} \approx 1.42$ while the position of the 1st maximum in $S_{AA}(q)$ occurs at $q \approx 7.2$.

VI. POTENTIAL ENERGIES AND PRESSURES OF THE PARENT AND INHERENT STRUCTURES

In Fig. 11 we show how the potential energies per particle of the parent and inherent structures depend on the temperature. In all panels the same data are presented, but on different scales. The results shown in this figure can be compared, for example, with the data in Fig. 1 of

Ref.[34].

To produce the inherent structures we used the FIRE algorithm [50, 51] within the LAMMPS program [47, 49]. The criterion for the convergence of the minimization process was: the change in the total potential energy in a particular step has to be smaller than 10^{-4} of the energy value. A maximum number of 10^4 steps was allowed. The value of the time step used was $dt = 0.002$. The recommended time step for the FIRE algorithm is the same as the time step used in MD simulations [49].

Every point in the shown plots originates from 1000 configurations of 8000 particles. These 1000 configurations originate from 10 independent runs, as described in this SM in the section on simulation procedure.

In Fig. 11, as in Fig. 1 of Ref.[34], we see that for $T > 1.5$ the average energies of the inherent structures, essentially, do not depend on the temperature.

Then, as the temperature of the parent system decreases, at $T \approx 1.0$, there occurs a crossover to the potential energy landscape (PEL) influenced regime.

Then, the figure shows that, at $T \approx 0.36$, the timescale of our relaxation procedure of the parent structures is absolutely not sufficient to capture the structural relaxation of the system.

In Fig. 12 we show the temperature dependencies of the pressure of parent and inherent structures. In principle, the behavior of all shown curves is similar to the behavior of the curves shown in Fig. 11. An interesting point to note, is that the pressure of the inherent structures becomes negative at $T \approx 0.8\epsilon$.

Thus, at $T < 0.8\epsilon$, the inherent structures should exhibit a tendency for the formation of cavities. The issue if the cavities and inhomogeneities in the inherent structures has been discussed in the past. See, for example, Ref.[53–55, 57–59]. In particular, for the Kob-Andersen system, it has been shown that, for the reduced densities $\rho\sigma^3 > 1.08$, the inherent structures remain homogeneous even when the pressure in these structures is negative (tensile). Thus, the crossover in the number of chains that we observe on the inherent structures is not associated with the formation of cavities.

VII. MEAN SQUARE DISPLACEMENT, DIFFUSION, INTERMEDIATE SELF-SCATTERING FUNCTION, AND α -RELAXATION TIME

A. Mean square displacement

Panel (a) of Fig.13 shows the dependencies of the mean square displacements (MSD) of the A -particles on time for selected temperatures. The behavior of the shown curves is well known from previous publications, for example from Fig.2 of Ref.[32]. Each curve shows the results from several simulations with different time-intervals for saving the values of the MSDs (LAMMPS's output). This is not noticeable in the curves corresponding to high temperatures. On the other hand, the curves at low temperatures exhibit significant fluctuations at large times. To reduce these fluctuations, the averaging over several runs has been performed. For example, for the red curve corresponding to $T = 0.45\epsilon$, several sets of runs have been made. For this reason, there are two red curves corresponding to $T = 0.45\epsilon$. The behavior of the MSDs curves at large times was used to determine the diffusion coefficient according to the formula $D = \langle (\Delta r)^2 \rangle / (6t)$. The dependence of (T/D) is shown in panel (c) of Fig.13 with the blue curve. The blue points were obtained from the MSDs at the largest available time. The blue line simply connects the blue points.

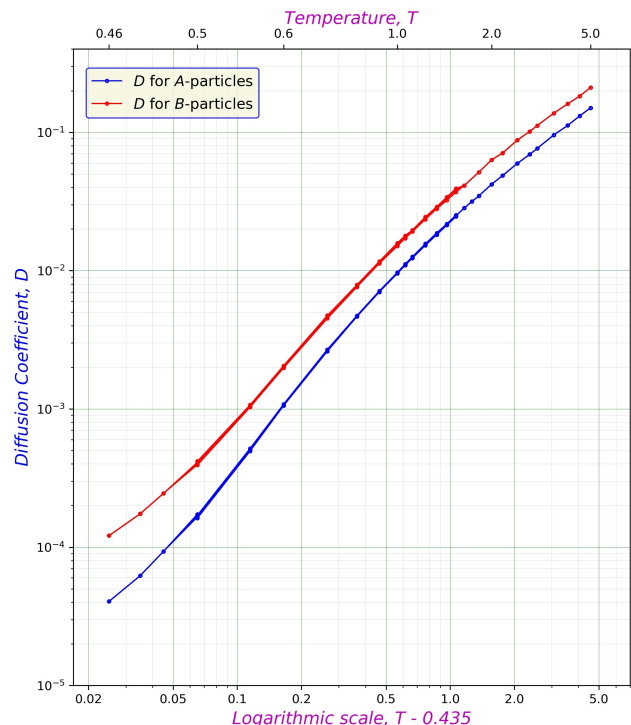


FIG. 14. This figure is for comparison with Fig.3 of Ref. [32]. Even though the curves look quite similar, there appear to be numerical differences which we cannot explain. Maybe, these discrepancies originate in the small differences between the used potentials.

B. Intermediate self-scattering function

Panel (b) of Fig.13 shows the dependencies of the intermediate self-scattering function (ISSF) on time at selected temperatures. In practice, we calculated the dependence on the time of the spherically averaged ISSF:

$$F(q_{max}, t) \equiv \left\langle \frac{\sin(x)}{x} \right\rangle_{i, t_0}, \quad (14)$$

where

$$x \equiv q_{max} |\vec{r}_i(t_o + t) - \vec{r}_i(t_o)|, \quad (15)$$

and the averaging in (14) is done over all particles A in the system and over a set of initial times, t_o . The value of q_{max} corresponds to the position of the 1st peak in the intermediate self-scattering function $S_{AA}(q)$ (11,13) from Fig. 9. Thus, $q_{max} \approx 7.23$. We note that in Ref. [33] the value of $q_{max} = 7.25$ was used. Our system is larger than the system used in Ref. [33]. We also used a slightly different form of the potential. In Ref. [34] the value of $q_{max} = 7.22$ was used (1372 particles). In Ref. [36] the value of $q_{max} = 7.0$ was used (1000 particles).

The value of τ_α can be determined either through fitting of the long-time behavior of the ISSF with the stretched-exponential function, as it has been done, for example, in

[56, 60], or, in a simpler way, by assuming that the value of τ_α corresponds to the time at which the ISSF decays to the value of $1/e$, as it has been done, for example, in Ref.[61]. In our work we used the second simpler approach. In panel (b) of Fig. 13 the value of $1/e$ is shown as the pink horizontal line.

In panel (c) of Fig. 13 we show the values of τ_α corresponding to the intersections of the horizontal line in Fig. 13(b) with the ISSF curves. These are the red circles. The red curve in Fig. 13(c) simply connects the red circles.

In Ref. [56] the value of τ_α was determined by fitting the large-time behaviors of the ISSFs with the stretched exponential functions. Then, the dependence of τ_α on temperature was fitted, for $T > 1.0$, with an exponential function, $\tau_\alpha(T) = \tau_\infty \exp(-E_\infty/T)$. The fitting parameters were: $\tau_\infty = 0.0693$ and $E_\infty = 2.91$. This function is shown as a green line segment in panel (c) of Fig. 13. We used the same exponential form, as described above, to fit our data at high temperatures. The result of the fit is shown with the blue line segment in Fig. 13(c). The corresponding values of the parameters are: $\tau_\infty = 0.105$ and $E_\infty = 2.40$.

The behavior of τ_α at low temperatures, $T < 1.0$, was fitted in Ref.[56] with the Vogel–Fulcher–Tammann (VFT) function: $\tau_\alpha(T) = \tau_\infty^{lowT} \exp[\mathcal{D}T_o/(T - T_o)]$. The values of parameters were: fragility parameter, $\mathcal{D} = 7.48$. VFT temperature, $T_o = 0.325$. The value of τ_∞^{lowT} ensured the continuity of the fit at $T = 1.0$. We used the same functional form to fit our data. The values of our parameters are: $\tau_\infty^{lowT} = 0.244$, $\mathcal{D} = 3.342$, and $T_o = 0.3229$. This fitting function is shown with the thick black curve.

We also would like to note that our data for the tem-

peratures $T < 0.48$ can be fitted with the simple exponential function: $\tau_\alpha = \exp[(13.84/T) - 23.71]$. This curve is shown as the magenta line in Fig. 13(c). In this context, see Ref.[43].

VIII. PLOT OF THE DIFFUSION COEFFICIENTS FOR A COMPARISON

In Fig. 14, we plot the dependencies on the temperature of the diffusion coefficients for A and B particles in a particular form, identical to the one used in Fig. 3 of Ref. [32]. The purpose of the figure is to provide yet another comparison with the previously obtained results. The data were obtained in the same way as the data on diffusion in panel (c) of Fig. 13.

IX. DISTRIBUTIONS OF THE POTENTIAL ENERGIES OF THE PARTICLES FORMING THE CHAINS

In Fig. 15 we show the probability distributions of the potential energies of the individual A -particles forming the chains. This figure is an extended version of Fig. 4 in the paper.

It follows from the figure that at $T = 1.0$ there are no differences in the distributions of the potential energies of the particles forming the chains and the distributions of potential energies of all A -particles. On the other hand, at $T = 0.05$ the differences between the two types of distributions are quite significant. This also can be seen from panel (d) of Fig. 4.

-
- [1] C.P. Royall and S.R. Williams. The role of local structure in dynamical arrest. *Phys. Rep.*, 560:1–75, 2015.
 - [2] H. Tanaka, H. Tong, R. Shi, and J. Russo. Revealing key structural features hidden in liquids and glasses. *Nat. Rev. Phys.*, 1(5):333–348, 2019.
 - [3] F. Lehmkuhler, B. Hankiewicz, M.A. Schroer, L. Müller, B. Ruta, D. Sheyfer, M. Sprung, K. Tono, T. Katayama, M. Yabashi, et al. Slowing down of dynamics and orientational order preceding crystallization in hard-sphere systems. *Sci. Adv.*, 6(43):eabc5916, 2020.
 - [4] E. Boattini, F. Smalenburg, and L. Filion. Averaging local structure to predict the dynamic propensity in supercooled liquids. *Phys. Rev. Lett.*, 127(8):088007, 2021.
 - [5] H. Tanaka. Roles of liquid structural ordering in glass transition, crystallization, and water’s anomalies. *J. Non-Cryst Solids: X*, 13:100076, 2022.
 - [6] J. Russo and H. Tanaka. Crystal nucleation as the ordering of multiple order parameters. *J. Chem. Phys.*, 145(21):211801, 2016.
 - [7] E. Sanz, C. Valeriani, E. Zaccarelli, W.C.K. Poon, M.E. Cates, and P.N. Pusey. Avalanches mediate crystallization in a hard-sphere glass. *PNAS*, 111(1):75–80, 2014.
 - [8] S. Jungblut and C. Dellago. Pathways to self-organization: Crystallization via nucleation and growth. *Eur. Phys. J. E*, 39(8):1–38, 2016.
 - [9] Y.-C. Hu, Y.-W. Li, Y. Yang, P.-F. Guan, H.-Y. Bai, and W.-H. Wang. Configuration correlation governs slow dynamics of supercooled metallic liquids. *PNAS*, 115(25):6375–6380, 2018.
 - [10] T.S. Ingebrigtsen, J.C. Dyre, T.B. Schröder, and C.P. Royall. Crystallization instability in glass-forming mixtures. *Phys. Rev. X*, 9(3):031016, 2019.
 - [11] S. Marín-Aguilar, H.H. Wensink, G. Foffi, and F. Smalenburg. Tetrahedrality dictates dynamics in hard sphere mixtures. *Phys. Rev. Lett.*, 124(20):208005, 2020.
 - [12] V.A. Levashov, R.E. Ryltsev, and N.M. Chtchelkatchev. Investigation of the degree of local structural similarity between the parent-liquid and children-crystal states for a model soft matter system. *Phys. A: Stat. Mech. Appl.*, 585:126387, 2022.
 - [13] V.A. Levashov, R.E. Ryltsev, and N.M. Chtchelkatchev. Structure of the simple harmonic-repulsive system in liquid and glassy states studied by the triple correlation function. *J. Condens. Matter Phys.*, 33(2):025403, 2020.

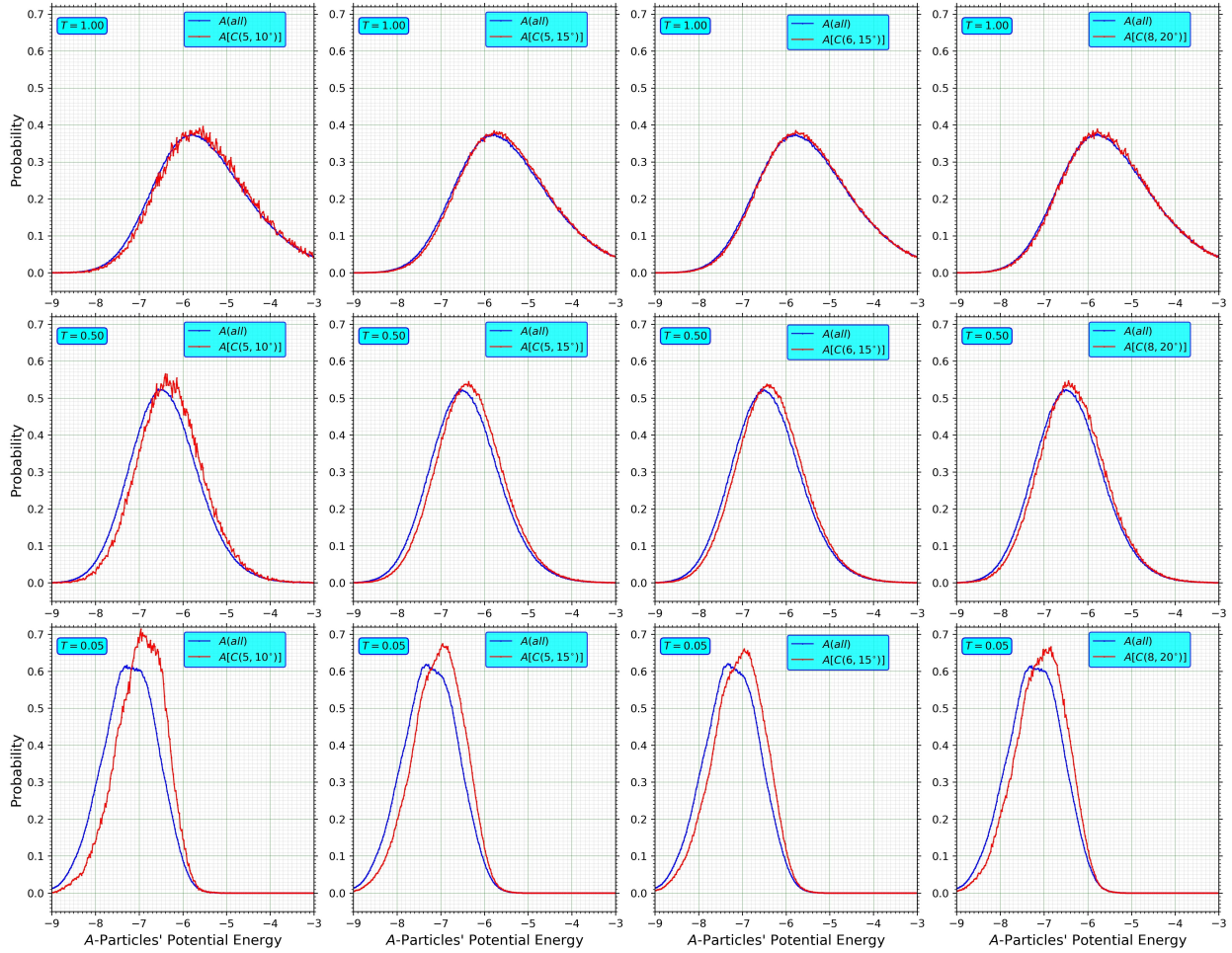


FIG. 15. The probability distributions of the potential energies of individual A -particles forming the chains. Each column in the figure shows the results for a chain of a particular type. The results for different temperatures are shown in different rows.

- [14] C.P. Royall, F. Turci, and T. Speck. Dynamical phase transitions and their relation to structural and thermodynamic aspects of glass physics. *J. Chem. Phys.*, 153(9):090901, 2020.
- [15] J.D. Bernal. A geometrical approach to the structure of liquids. *Nature*, 183(4655):141–147, 1959.
- [16] P.J. Steinhardt, D.R. Nelson, and M. Ronchetti. Bond-orientational order in liquids and glasses. *Phys. Rev. B*, 28:784, 1983.
- [17] T. Egami and D. Srolovitz. Local structural fluctuations in amorphous and liquid metals: a simple theory of the glass transition. *J. Phys. F: Met. Phys.*, 12(10):2141, 1982.
- [18] A. Malins, J. Eggers, H. Tanaka, and C.P. Royall. Lifetimes and lengthscales of structural motifs in a model glassformer. *Faraday Discuss.*, 167:405–423, 2013.
- [19] Z.W. Wu, M.Z. Li, W.H. Wang, and K.X. Liu. Hidden topological order and its correlation with glass-forming ability in metallic glasses. *Nat. Commun.*, 6(1):1–7, 2015.
- [20] H.W. Sheng, W.K. Luo, F.M. Alamgir, J.M. Bai, and E. Ma. Atomic packing and short-to-medium-range order in metallic glasses. *Nature*, 439(7075):419–425, 2006.
- [21] S.P. Pan, J.Y. Qin, W.M. Wang, and T.K. Gu. Origin of splitting of the second peak in the pair-distribution function for metallic glasses. *Phys. Rev. B*, 84(9):092201, 2011.
- [22] J.-P. Bouchaud and G. Biroli. On the Adam-Gibbs-Kirkpatrick-Thirumalai-Wolynes scenario for the viscosity increase in glasses. *J. Chem. Phys.*, 121(15):7347–7354, 2004.
- [23] L. Berthier and W. Kob. Static point-to-set correlations in glass-forming liquids. *Phys. Rev. E*, 85(1):011102, 2012.
- [24] C.W. Ryu and T. Egami. Medium-range atomic correlation in simple liquids. I. Distinction from short-range order. *Phys. Rev. E*, 104(6):064109, 2021.
- [25] I. Tah and S. Karmakar. Kinetic fragility directly correlates with the many-body static amorphous order in glass-forming liquids. *Phys. Rev. Mater.*, 6(3):035601, 2022.
- [26] V.A. Levashov. Contribution to viscosity from the structural relaxation via the atomic scale green-kubo stress correlation function. *J. Chem. Phys.*, 147(18):184502, 2017.
- [27] X. Fan, Y. Sun, C.-Z. Wang, K.-M. Ho, M.S. Altman, and L. Huang. Unveiling the medium-range order in glass

- models and its role in glass formation. *Phys. Rev. B*, 101(21):214104, 2020.
- [28] Z. Zhang and W. Kob. Revealing the three-dimensional structure of liquids using four-point correlation functions. *PNAS*, 117(25):14032–14037, 2020.
- [29] H. Yuan, Z. Zhang, W. Kob, and Y. Wang. Connecting packing efficiency of binary hard sphere systems to their intermediate range structure. *Phys. Rev. Lett.*, 127(27):278001, 2021.
- [30] E. Boattini, S. Marín-Aguilar, S. Mitra, G. Foffi, F. Smalenburg, and L. Filion. Autonomously revealing hidden local structures in supercooled liquids. *Nat. Commun.*, 11(1):1–9, 2020.
- [31] A. Banerjee, M. Sevilla, J.F. Rudzinski, and R. Cortes-Huerto. Attractive interactions lead to long-range structures in model supercooled liquids. *ArXiv preprint ArXiv:2107.04478*, 2021.
- [32] W. Kob and H.C. Andersen. Testing mode-coupling theory for a supercooled binary Lennard-Jones mixture I: The van hove correlation function. *Phys. Rev. E*, 51(5):4626, 1995.
- [33] W. Kob and H.C. Andersen. Testing mode-coupling theory for a supercooled binary Lennard-Jones mixture. II. intermediate scattering function and dynamic susceptibility. *Phys. Rev. E*, 52(4):4134, 1995.
- [34] S. Sastry, P.G. Debenedetti, and F.H. Stillinger. Signatures of distinct dynamical regimes in the energy landscape of a glass-forming liquid. *Nature*, 393(6685):554–557, 1998.
- [35] A. Mukherjee, S. Bhattacharyya, and B. Bagchi. Pressure and temperature dependence of viscosity and diffusion coefficients of a glassy binary mixture. *J. Chem. Phys.*, 116(11):4577–4586, 2002.
- [36] D. Coslovich. Locally preferred structures and many-body static correlations in viscous liquids. *Phys. Rev. E*, 83(5):051505, 2011.
- [37] W. Kob, C. Donati, S.J. Plimpton, P.H. Poole, and S.C. Glotzer. Dynamical heterogeneities in a supercooled Lennard-Jones liquid. *Phys. Rev. Lett.*, 79(15):2827, 1997.
- [38] C. Donati, J.F. Douglas, W. Kob, S.J. Plimpton, P.H. Poole, and S.C. Glotzer. Stringlike cooperative motion in a supercooled liquid. *Phys. Rev. Lett.*, 80(11):2338, 1998.
- [39] G. Biroli, J.-P. Bouchaud, A. Cavagna, T.S. Grigera, and P. Verrocchio. Thermodynamic signature of growing amorphous order in glass-forming liquids. *Nat. Phys.*, 4(10):771–775, 2008.
- [40] L. Berthier and G. Tarjus. Nonperturbative effect of attractive forces in viscous liquids. *Phys. Rev. Lett.*, 103(17):170601, 2009.
- [41] A. Malins, S.R. Williams, J. Eggers, and C.P. Royall. Identification of structure in condensed matter with the topological cluster classification. *J. Chem. Phys.*, 139(23):234506, 2013.
- [42] D. Coslovich. Static triplet correlations in glass-forming liquids: A molecular dynamics study. *J. Chem. Phys.*, **138**:12A539, 2013.
- [43] P. Das and S. Sastry. Crossover in dynamics in the kob-andersen binary mixture glass-forming liquid. *J. Non. Cryst. Solids: X*, 14:100098, 2022.
- [44] G. Wahnström. Molecular-dynamics study of a supercooled two-component Lennard-Jones system. *Phys. Rev. A*, 44(6):3752, 1991.
- [45] A. Malins, J. Eggers, C.P. Royall, S.R. Williams, and H. Tanaka. Identification of long-lived clusters and their link to slow dynamics in a model glass former. *J. Chem. Phys.*, 138(12):12A535, 2013.
- [46] S.D. Stoddard and J. Ford. Numerical experiments on the stochastic behavior of a Lennard-Jones gas system. *Phys. Rev. A*, 8(3):1504, 1973.
- [47] S. Plimpton. Fast parallel algorithms for short-range molecular dynamics. *J. Comp. Phys.*, **117**:1, 1995.
- [48] A.P. Thompson, H.M. Aktulga, R. Berger, D.S. Bolintineanu, W.M. Brown, P.S. Crozier, P.J. in’t Veld, A. Kohlmeyer, S.G. Moore, T.D. Nguyen, et al. LAMMPS—a flexible simulation tool for particle-based materials modeling at the atomic, meso, and continuum scales. *Comput. Phys. Commun.*, 271:108171, 2022.
- [49] LAMMPS molecular dynamics simulator. <https://www.lammps.org>. Accessed June 2022.
- [50] E. Bitzek, P. Koskinen, F. Gähler, M. Moseler, and P. Gumbsch. Structural relaxation made simple. *Phys. Rev. Lett.*, 97(17):170201, 2006.
- [51] J. Guérolé, W.G. Nöhling, A. Vaid, F. Houllé, Z. Xie, A. Prakash, and E. Bitzek. Assessment and optimization of the fast inertial relaxation engine (fire) for energy minimization in atomistic simulations and its implementation in lammps. *Comput. Mater. Sci.*, 175:109584, 2020.
- [52] S. Toxvaerd and J.C. Dyre. Communication: Shifted forces in molecular dynamics. *J. Chem. Phys.*, 134(8):081102, 2011.
- [53] S. Sastry. Liquid limits: Glass transition and liquid-gas spinodal boundaries of metastable liquids. *Phys. Rev. Lett.*, 85(3):590, 2000.
- [54] Y.E. Altabet, A.L. Fenley, F.H. Stillinger, and P.G. Debenedetti. Cavitation transition in the energy landscape: Distinct tensile yielding behavior in strongly and weakly attractive systems. *J. Chem. Phys.*, 148(11):114501, 2018.
- [55] M.A. Makeev and N.V. Priezjev. Distributions of pore sizes and atomic densities in binary mixtures revealed by molecular dynamics simulations. *Phys. Rev. E*, 97(2):023002, 2018.
- [56] A. Malins, J. Eggers, H. Tanaka, and C.P. Royall. Lifetimes and lengthscales of structural motifs in a model glassformer. *Faraday Discuss.*, 167:405–423, 2013.
- [57] S. Sastry, P.G. Debenedetti, and F.H. Stillinger. Statistical geometry of particle packings. ii. “weak spots” in liquids. *Phys. Rev. E*, 56(5):5533, 1997.
- [58] J. Hernández-Rojas and D.J. Wales. Density effects in a bulk binary Lennard-Jones system. *Phys. Rev. B*, 68(14):144202, 2003.
- [59] Y.E. Altabet, F.H. Stillinger, and P.G. Debenedetti. A cavitation transition in the energy landscape of simple cohesive liquids and glasses. *J. Chem. Phys.*, 145(21):211905, 2016.
- [60] V.A. Levashov, J.R. Morris, and T. Egami. The origin of viscosity as seen through atomic level stress correlation function. *J. Chem. Phys.*, 138(4):044507, 2013.
- [61] U.R. Pedersen, T.B. Schröder, and J.C. Dyre. Repulsive reference potential reproducing the dynamics of a liquid with attractions. *Phys. Rev. Lett.*, 105(15):157801, 2010.